



3D-FV-FE Aeroacoustic Larynx Model for Investigation of Functional Based Voice Disorders

Sebastian Falk^{1*}, Stefan Kniesburges¹, Stefan Schoder², Bernhard Jakubaß¹, Paul Maurerlehner², Matthias Echternach³, Manfred Kaltenbacher² and Michael Döllinger¹

¹ Division of Phoniatics and Pediatric Audiology, Department of Otorhinolaryngology, Head & Neck Surgery, Friedrich-Alexander-University Erlangen-Nürnberg, Erlangen, Germany, ² Institute of Fundamentals and Theory in Electrical Engineering, Division Vibro- and Aeroacoustics, Graz University of Technology, Graz, Austria, ³ Division of Phoniatics and Pediatric Audiology, Department of Otorhinolaryngology, Munich University Hospital (LMU), Munich, Germany

OPEN ACCESS

Edited by:

Rajat Mittal,
Johns Hopkins University,
United States

Reviewed by:

Byron Erath,
Clarkson University, United States
Haoxiang Luo,
Vanderbilt University, United States
Xudong Zheng,
University of Maine, United States

*Correspondence:

Sebastian Falk
sebastian.falk@uk-erlangen.de

Specialty section:

This article was submitted to
Computational Physiology and
Medicine,
a section of the journal
Frontiers in Physiology

Received: 13 October 2020

Accepted: 09 February 2021

Published: 08 March 2021

Citation:

Falk S, Kniesburges S, Schoder S, Jakubaß B, Maurerlehner P, Echternach M, Kaltenbacher M and Döllinger M (2021) 3D-FV-FE Aeroacoustic Larynx Model for Investigation of Functional Based Voice Disorders.
Front. Physiol. 12:616985.
doi: 10.3389/fphys.2021.616985

For the clinical analysis of underlying mechanisms of voice disorders, we developed a numerical aeroacoustic larynx model, called *simVoice*, that mimics commonly observed functional laryngeal disorders as glottal insufficiency and vibrational left-right asymmetries. The model is a combination of the Finite Volume (FV) CFD solver Star-CCM+ and the Finite Element (FE) aeroacoustic solver CFS++. *simVoice* models turbulence using Large Eddy Simulations (LES) and the acoustic wave propagation with the perturbed convective wave equation (PCWE). Its geometry corresponds to a simplified larynx and a vocal tract model representing the vowel /a/. The oscillations of the vocal folds are externally driven. In total, 10 configurations with different degrees of functional-based disorders were simulated and analyzed. The energy transfer between the glottal airflow and the vocal folds decreases with an increasing glottal insufficiency and potentially reflects the higher effort during speech for patients being concerned. This loss of energy transfer may also have an essential influence on the quality of the sound signal as expressed by decreasing sound pressure level (SPL), Cepstral Peak Prominence (CPP), and Vocal Efficiency (VE). Asymmetry in the vocal fold oscillations also reduces the quality of the sound signal. However, *simVoice* confirmed previous clinical and experimental observations that a high level of glottal insufficiency worsens the acoustic signal quality more than oscillatory left-right asymmetry. Both symptoms in combination will further reduce the quality of the sound signal. In summary, *simVoice* allows for detailed analysis of the origins of disordered voice production and hence fosters the further understanding of laryngeal physiology, including occurring dependencies. A current walltime of 10 h/cycle is, with a prospective increase in computing power, auspicious for a future clinical use of *simVoice*.

Keywords: computational fluid dynamics, computational aero acoustics, glottal insufficiency, left-right asymmetry, posterior gap, *simVoice* (numerical larynx model)

1. INTRODUCTION

The human voice as a prerequisite for speech production is our most important tool to communicate with other people. Moreover, people heavily rely on oral communication in their professional life. Disorders of the ordinary communication system have severe consequences on concerned persons' employments and even on the whole economic system (Ruben, 2000). The phonatory process, the prerequisite for human speech, describes the production of the human voice and depends on various factors as age, gender, training, and health status (Titze, 2000; Aronson and Bless, 2009).

The human voice results from a periodic oscillation of the vocal folds (VF) in the larynx, see **Figure 1**. The oscillations are caused by a complex fluid-structure interaction between the tracheal airflow and the elastic tissue of the vocal folds. Thereby, the airflow is the main sound generating source, that is subsequently modulated by the vocal tract consisting of the upper airway structures and is then emitted from the lips as an audible signal.

This process is supposed to be most efficient when (1) the vocal folds close the gap in between (called glottis) completely in each oscillation cycle and (2) when they oscillate symmetrically and periodic (Titze, 2000). An incomplete glottis closure or glottal insufficiency and asymmetric oscillations of the vocal folds cause a reduced voice quality with decreased tonal and increased broadband sound in the voice signal (Park and Mongeau, 2008; Hoffman et al., 2012; Yamauchi et al., 2016). The voice is then described as aspirated/breathy and hoarse. However, as shown by Inwald et al. (2010) and Schneider and Bigenzahn (2003), these underlying symptoms do not only occur in pathologic (e.g., scars, paresis, or paralysis) cases (Bhatt and Verma, 2014), but also in apparently organically healthy larynges (Rammage et al., 1992; Inwald et al., 2010; Patel et al., 2012) and with advancing age of the patients (Södersten et al., 1995; Vaca et al., 2017).

The scientific investigation and the clinical diagnostics suffer from the restricted location of the vocal folds inside the larynx, especially during phonation. To compensate this restriction, experimental (*ex/in vivo*), and numerical models have been

developed. *In vivo* studies on glottal insufficiency were done by Södersten et al. (1995), Södersten and Lindestad (1990), and Yamauchi et al. (2014) and on the asymmetric vocal fold oscillations by Eysholdt et al. (2003). Whereas *in vivo* studies are difficult to perform and are mainly restricted to pure observation of the vocal fold oscillations (Inwald et al., 2010; Döllinger et al., 2012), *ex vivo* experiments with excised cadaver larynges (e.g., canine, porcine, human) provide better access to the laryngeal area and enable to manipulate the larynx (Hoffman et al., 2012; Birk et al., 2017b). *Ex vivo* studies about different levels of glottal insufficiency were reported by Döllinger et al. (2018) and Thornton et al. (2019) using rabbit larynges and Birk et al. (2017b) who used porcine larynges. Moreover, Oren et al. (2016) investigated asymmetric vocal fold oscillations in excised canine larynges.

Besides excised larynges, synthetic vocal fold models with silicone vocal folds were carried out with the focus on the glottal insufficiency (Park and Mongeau, 2008; Kirmse et al., 2010; Kniesburges et al., 2013, 2016). Pickup and Thomson (2009) and Zhang et al. (2012) investigated asymmetric vocal fold oscillations with a silicone model. Such models can mimic specific physiological and disordered motion patterns of the vocal folds for which they have been developed for and are therefore well-established in voice science (Zhang et al., 2004; Thomson et al., 2005; Park and Mongeau, 2008; Kirmse et al., 2010; Murray and Thomson, 2012; Kniesburges et al., 2013, 2016; Van Hirtum and Pelorson, 2017; Motie-Shirazi et al., 2019; Taylor et al., 2019; Romero et al., 2020). However, both *ex vivo* and synthetic larynx models are restricted regarding the spatial resolution of the measuring data of fluid flow, the vocal fold dynamics, and their interaction.

Thus, numerical models based on Finite-Elements and/or Finite-Volumes have great potential to be applied in the clinical routine, e.g., diagnostics and treatment control. Numeric simulations, regarding the effect of the glottal insufficiency on the human voice, were done by Zörner et al. (2016) and on the asymmetric vocal fold oscillations by Xue et al. (2010) and Samlan et al. (2014). In contrast to experimental models, computer models provide the complete 3D data of the flow field

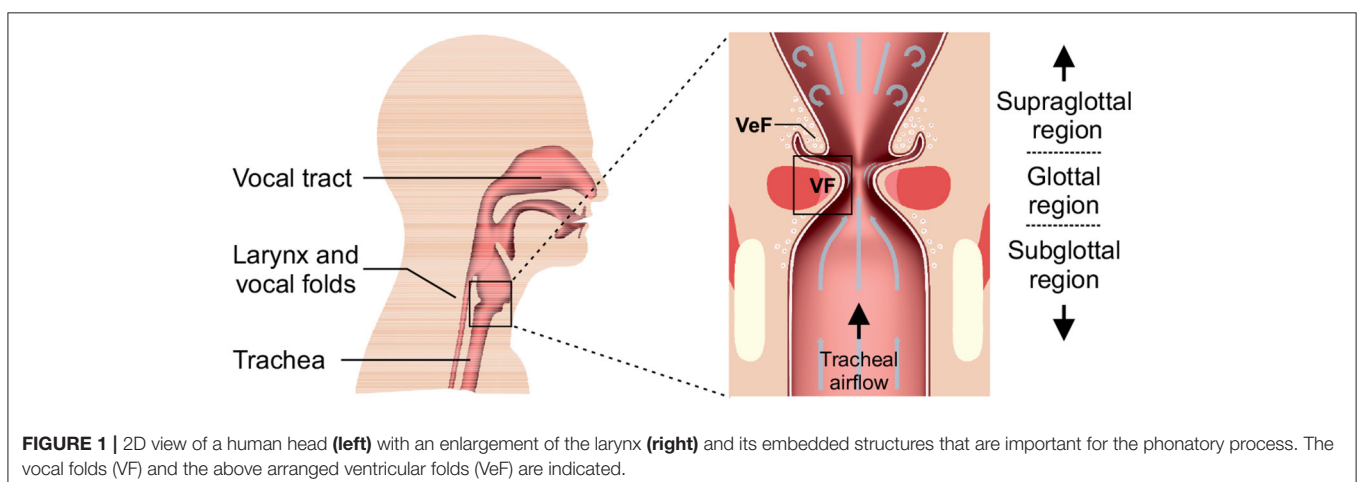


TABLE 1 | Parameter reported for normal male phonation in *in vivo* and *ex vivo* studies compared with the experimental silicone model *synthVOICE* (Kniesburges et al., 2013, 2016, 2020; Kniesburges, 2014) (validation cases) and the performed numerical validation simulations by *simVoice* (Sadeghi et al., 2018, 2019a,b; Sadeghi, 2019; Schoder et al., 2020).

Parameter	<i>In vivo</i> (male)	<i>Ex vivo</i> (male)	Silicone model (<i>synthVOICE</i>)	Numerical simulation (<i>simVoice</i>)
Fundamental Frequency (F_0) [Hz]	103–220 (Larsson and Hertegård, 2004; Sundberg et al., 2005)	97–200 (Döllinger et al., 2005, 2016; Döllinger and Berry, 2006b)	148	148
Vocal fold length (anterior–posterior) [mm]	14–17 (Schuberth et al., 2002; Hoppe et al., 2003; Larsson and Hertegård, 2004; Rogers et al., 2014)	13–18 (Lagier et al., 2017)	15	15
Glottal gap diameter (d_G) [mm]	1.49–2.8 (Hoppe et al., 2003; George et al., 2008; Semmler et al., 2018)	2.3–5.6 (Döllinger et al., 2005, 2016; Döllinger and Berry, 2006a,b; Boessenecker et al., 2007)	4.66	4.66
Speed Quotient (SQ) [a.u.]	0.59–1.978 (Holmberg et al., 1988; Baken and Orlikoff, 2000)	0.8–1.6 (Döllinger et al., 2014)	0.67	0.67
Open Quotient (OQ) [a.u.]	0.37–1.00 (Holmberg et al., 1988; Baken and Orlikoff, 2000)	0.42–1.00 (Mendelsohn et al., 2015)	0.93	0.93
Mean flow rate (\bar{Q}) [$\frac{l}{min}$]	4.5–18 (Holmberg et al., 1988; Baken and Orlikoff, 2000)	6–108 (Döllinger et al., 2005, 2014, 2016; Döllinger and Berry, 2006a,b; Boessenecker et al., 2007)	65–115	37.8–132
Mean subglottal pressure (P_{sub}) [Pa]	157–3510 (Holmberg et al., 1988; Sundberg et al., 1993, 2005; Alku et al., 2006)	600–4300 (Döllinger et al., 2005, 2014, 2016; Döllinger and Berry, 2006b)	2449–3251	2450–3251

(Sciamarella and Le Quéré, 2008; Zörner et al., 2013; Sadeghi et al., 2018) and in case of coupled models the fluid-structure interaction (FSI) between flow, tissue and the aeroacoustic sound generation and propagation during phonation (de Oliveira Rosa et al., 2003; Luo et al., 2008, 2009; Tao and Jiang, 2008; Link et al., 2009; Kaltenbacher et al., 2014; Xue et al., 2014; Jo et al., 2016).

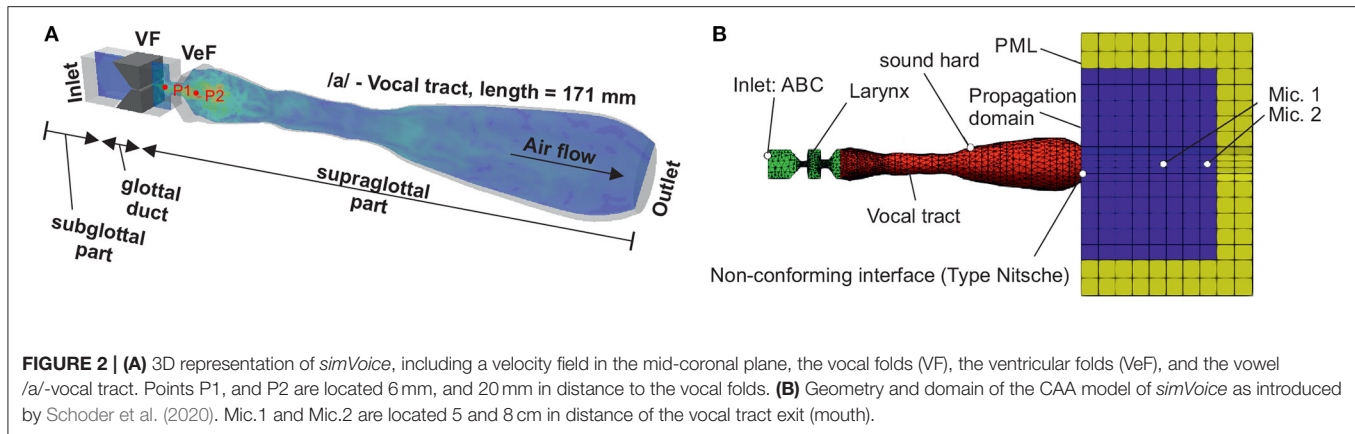
The large drawback of these numerical models are the large computational costs to perform the simulations (Sadeghi et al., 2018). Thus, they are not applicable in the clinical environment yet, where a short wall time with sufficient accuracy is needed. However, computational fluid dynamic (CFD) models with prescribed vocal fold movements and a prospective increasing computational power already keeps the simulation time adequately small (Sadeghi et al., 2019b).

For the development of our hybrid (sound propagation is calculated based on aeroacoustic source terms from the flow simulation) 3D aeroacoustic numeric larynx model *simVoice* (Sadeghi et al., 2018, 2019a,b; Schoder et al., 2020) for future clinic usefulness, it is essential to replicate normal and disordered glottal closures and dynamical asymmetries. A method to set up a workflow containing the import of various physiological and disordered glottal geometries into *simVoice* is shown in this study. We concentrate on modeling four disordered cases of glottal insufficiency based on high-speed video data of porcine *ex vivo* experiments performed by Birk et al. (2017b). Moreover, symmetric and asymmetric vocal fold motions are modeled. Our hypotheses for this study are:

- Hypothesis 1: Our existing and validated 3D-FV-FE numerical larynx model *simVoice* can accurately mimic and simulate realistic glottis geometries and vocal fold motions based on experimental high-speed video data.
- Hypothesis 2: *simVoice* can qualitatively and quantitatively mimic typical glottal parameters quantifying the different levels of glottal insufficiency that are reported in the literature.
- Hypothesis 3: Typical parameters of the acoustic voice signal computed from the simulated sound signal show typical characteristics for glottal insufficiency and asymmetric vocal fold oscillations.

2. METHODS: HYBRID AEROACOUSTIC NUMERICAL LARYNX MODEL – *SIMVOICE*

The 3D aeroacoustic numeric larynx model *simVoice* is a combination of the Finite Volume (FV) CFD solver Star-CCM+ and the Finite Element (FE) solver CFS++ (Kaltenbacher, 2015). The basic *simVoice* model was validated against a silicone model that provided an extensively large set of experimental data, including the vocal fold motion, the flow field, and produced sound field (Kniesburges et al., 2013, 2016, 2020; Lodermeier et al., 2015, 2018). Characteristic parameters of the silicone model performance and corresponding physiological male values are shown in **Table 1**. Validation parameters in detail were: (1) Flow dynamic properties as pressure measurements and the



velocity field with the glottal jet in the supraglottal region using particle image velocimetry (PIV) by Sadeghi et al. (2018, 2019a), and (2) the acoustic signal by Schoder et al. (2020). In this study, the investigated configurations of glottal insufficiency and asymmetric vocal fold oscillations are synthetic cases that were derived as combination from *ex vivo* (Birk et al., 2016, 2017a) and silicone model experiments (Kniesburges et al., 2013). Thus, there are no experimental data for validation purposes.

2.1. *simVoice* – CFD

2.1.1. Geometric Dimensions

The CFD model *simVoice* represents three main parts: the subglottal section upstream of the vocal folds, the glottal duct with the two vocal folds (VF) and the supraglottal part with the ventricular folds (VeF) and an MRI-based vocal tract (VT), see **Figure 2A**. The vocal folds are based on the well-known M5 model (Scherer et al., 2001; Thomson et al., 2005) and the numerical domain dimension is obtained from the experimental setup of a synthetic vocal fold model (Becker et al., 2009; Kniesburges et al., 2013, 2016; Loder Meyer et al., 2015). All dimensions of the larynx structures are in the human length scale (Titze, 2000). The basic development of *simVoice* is described in (Sadeghi et al., 2018, 2019a,b). The gap between the VeF is 5 mm as in (Sadeghi et al., 2019a). The vocal tract represents the vowel /a/ and was developed by Probst et al. (2019) based on MRI data of 6 professional tenors (Echternach et al., 2011). Probst et al. (2019) simplified the single tenors' VTs with the method introduced by Story et al. (1996) and generated a mean vocal tract model by averaging the six single vocal tracts. The resulting staged vocal tract model was subsequently smoothed with linear interpolation. Arnela et al. (2016) showed, that using a simplified vocal tract instead of a realistic vocal tract is an appropriate approach. The distance between the vocal folds and the outlet of the vocal tract is 171 mm.

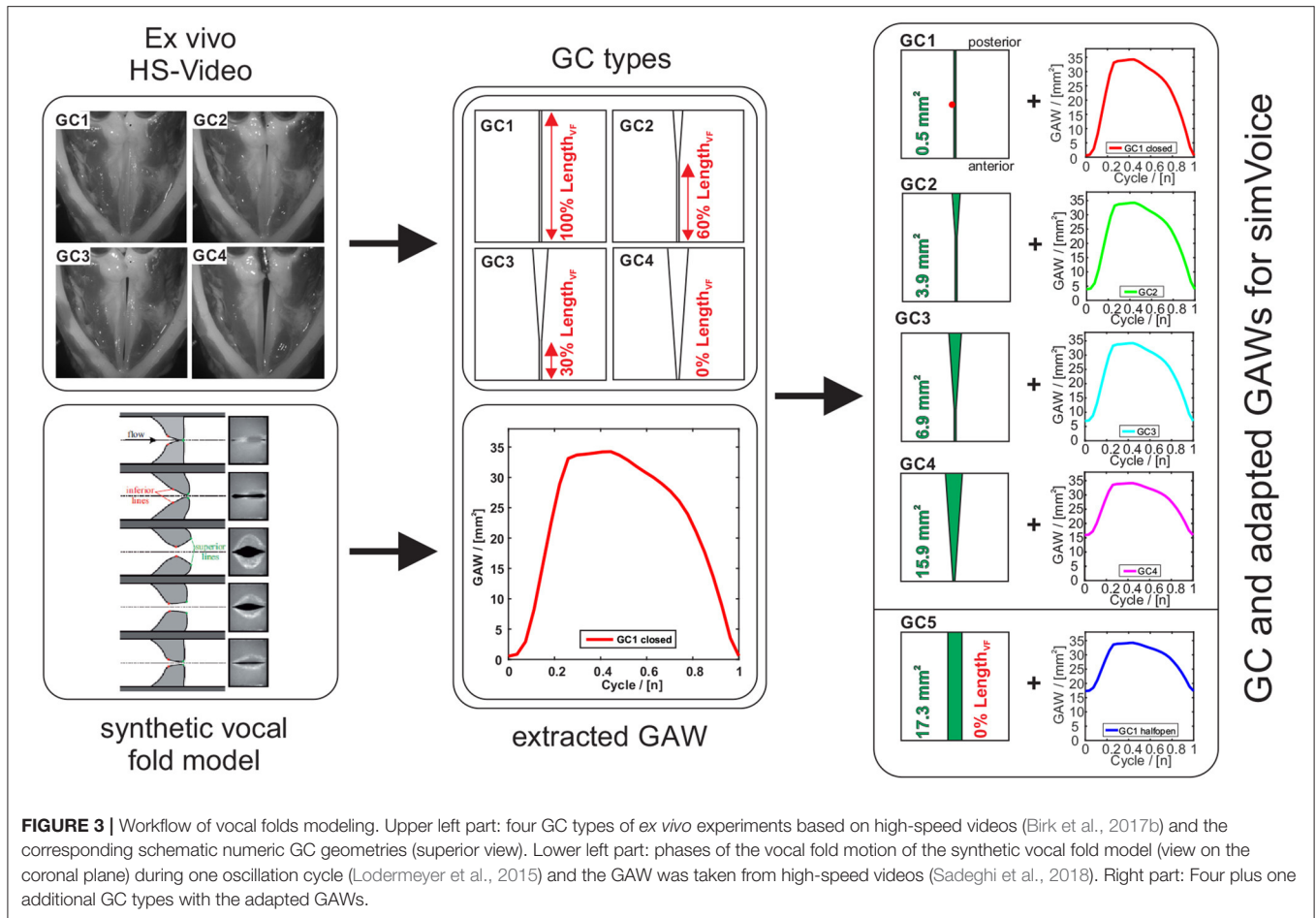
2.1.2. Modeling the Glottis Geometry

In this study, four types of clinically seen glottis closures (GC1 to GC4) were designed that are based on high-speed recordings obtained from experiments with *ex vivo* porcine larynges by Birk et al. (2016, 2017a), see **Figure 3**. Furthermore, an additional type GC5 with a rectangular glottis shape, similar

to a midmembranous gap (Södersten et al., 1995), was modeled. GC1 to GC4 represent posterior gaps with an increasing glottal insufficiency, whereas GC5 represents a complete glottal insufficiency. A glottal insufficiency can not only occur in pathological phonation cases as a result of scars, paresis, paralysis, or age-related atrophy (Bhatt and Verma, 2014; Vaca et al., 2017), but also in physiological phonation of women or children with a triangular-shaped gap located at the posterior part of the glottis (Södersten and Lindestad, 1990; Rammage et al., 1992; Södersten et al., 1995; Inwald et al., 2010; Döllinger et al., 2012; Patel et al., 2012). All GC types are modeled by two parameters: (1) the initial glottal gap area and (2) the length of the closed part of the glottis divided by the entire glottis length. As shown in **Figure 3**, the modeled glottis is either fully closed (GC1: 100% $Length_{VF}$), partly closed (GC2: 60% and GC3: 30% $Length_{VF}$), or completely open (GC4 and GC5: 0% $Length_{VF}$) at the initial glottal gap. The initial glottal gaps for GC2 to GC4 are based on the glottal gap index of Birk et al. (2016, 2017a) and the initial glottal gap of GC5 is half the maximum GAW of the synthetic model (Kniesburges et al., 2016). As described by Sadeghi et al. (2018), there must be a small area between both vocal folds of 0.5 mm^2 at GC1 to reach a numerically stable simulation. Nevertheless, this small gap still interrupts the flow through the glottis during the closed phase, as shown by Sadeghi et al. (2019b). For GC2, GC3, and GC4, the initial glottal gaps possess a triangular and for GC5 a rectangular shape, see **Figure 3**.

2.1.3. Vocal Fold Motion

The lower part of **Figure 3** shows the phases of the synthetic vocal folds during one oscillation cycle (Loder Meyer et al., 2015; Kniesburges et al., 2020) and the corresponding glottal area waveform (GAW). The GAW is computed as the change of glottal area over time and is a common measure for the description of laryngeal dynamics. Based on the GAW of the synthetic model (Kniesburges et al., 2016), the oscillation of the vocal folds is modeled in *simVoice* as proposed by Sadeghi et al. (2018). In the right part of **Figure 3**, the five GC types combined with the respective modified GAWs are shown. The GAW for GC1 is equal to that used by (Sadeghi et al., 2018). The GAWs for GC2 to GC5 were computed as follows:



$$A_i(t) = A_i^0 + \frac{A_0^{max} - A_i^0}{A_0^{max}} \cdot A_0(t) \quad (1)$$

where $A_i(t)$ is the modified GAW (of the individual GC type), subscript $i = 0$ indicates the GAW of the synthetic model of Kniesburges et al. (2016), and subscript $i = 1$ to 5 indicates GC1 to GC5. A_i^{max} is the maximum value of the GAW and A_i^0 represents the initial glottal gap area, see **Figure 3**.

We explicitly selected one motion pattern in combination with the five increasing levels of glottal insufficiency (GC1-GC5). With this strategy, we avoided to include individual effects of the patient-specific motion that may overlap the effects of the glottal insufficiency in the acoustic results.

To reduce the computational costs of the CFD simulations, the vocal fold dynamics are externally forced with characteristic dynamic patterns according to the modified GAWs. The computation of the elliptic shaped vocal fold motion is generated by a sinusoidal function along the two vocal folds (Sadeghi et al., 2018). Additionally, Sadeghi et al. (2018) added a simple convergent-divergent standard mucosal wave-like motion model based on experiments (time periods of convergent and divergent glottal duct shapes) and the literature for typical angles of the glottal duct during oscillation (Titze, 2000). It contains a convergent shaped glottal duct during the opening (0.1 T to

0.32 T) with an angle range of 0° to 5° and a divergent duct (0.32 T to 0.9 T) with angles of -10° to 0° . The glottis is closed between 0.9 T and 0.1 T of the next cycle. The 3D vocal fold motion is realized by moving wall boundaries of the vocal folds that form the glottal duct, see **Supplementary Video 1**. For all GC types, the vocal folds oscillate with a fundamental frequency of $f_0 = 148 \text{ Hz}$. The maximum glottis width of 4.66 mm is in the range as reported for *ex vivo* male larynx studies (up to 5.6 mm) (Döllinger et al., 2005; Döllinger and Berry, 2006a,b; Boessenecker et al., 2007) but higher than reported for *in vivo* measurements (up to 2.8 mm) (George et al., 2008; Semmler et al., 2018).

For the symmetric motion, both vocal folds move equally but in opposite directions. The left-right asymmetric vocal fold motion is realized by reducing the amplitude of one vocal fold to 50% (of the original amplitude), see **Figure 4** and **Supplementary Video 2**. Subsequently, the asymmetric motion reduces the corresponding maxima of the GAWs to 75% compared to the symmetric cases.

2.1.4. Boundary Conditions

At all walls of the *simVoice* model, no-slip no-injection boundary conditions were applied. The walls of the moving vocal folds were defined as moving wall boundaries. For all simulation cases, the

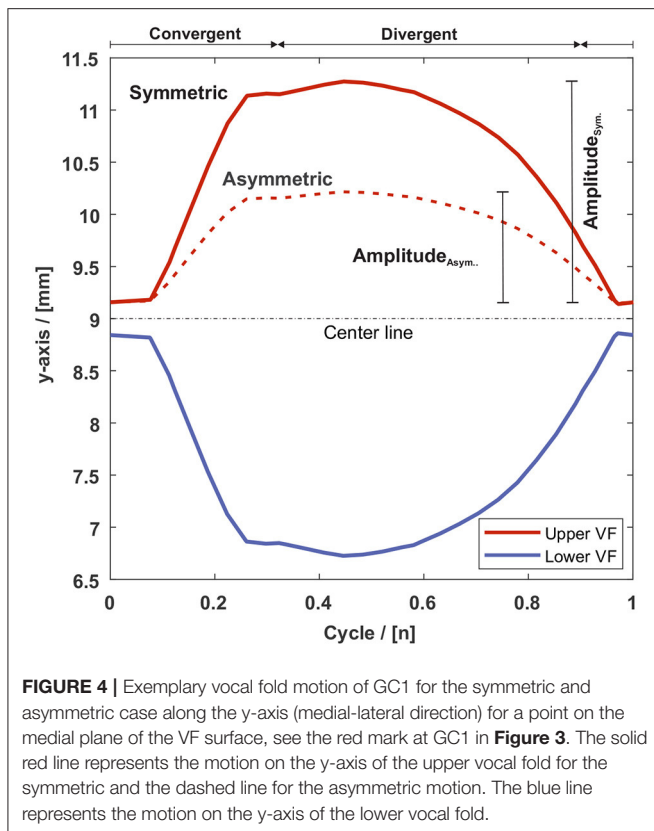


FIGURE 4 | Exemplary vocal fold motion of GC1 for the symmetric and asymmetric case along the y-axis (medial-lateral direction) for a point on the medial plane of the VF surface, see the red mark at GC1 in **Figure 3**. The solid red line represents the motion on the y-axis of the upper vocal fold for the symmetric and the dashed line for the asymmetric motion. The blue line represents the motion on the y-axis of the lower vocal fold.

mean pressure of the subglottal inlet boundary is $P_{inlet} = 775\text{Pa}$ that is in the physiologic range of human lunge pressures during normal phonation (Titze, 2000). The mean pressure at the outlet, which represents the mouth, is $P_{outlet} = 0\text{Pa}$. The kinematic viscosity of air was specified as $\nu = 1.5666 \cdot 10^{-5} \frac{\text{m}^2}{\text{s}}$ and the density of air constant at $\rho = 1.18415 \frac{\text{kg}}{\text{m}^3}$ as the Mach number is $Ma < 0.3$ (Kniesburgers et al., 2011).

2.1.5. Numerical Methods

The numerical setup is identical to the previous studies (Sadeghi et al., 2018, 2019a,b). To perform the simulations of *simVoice*, we use the software package STAR-CCM+ (Siemens, PLM Software, Plano, TX, USA) with a finite-volume cell-centered non-staggered grid. For modeling the turbulence, Large Eddy Simulations (LES) in combination with a Wall-Adapting Local Eddy-Viscosity (WALE) subgrid-scale model (Nicoud and Ducros, 1999) were carried out. The convective and diffusive terms of the Navier-Stokes equations were discretized with a central difference scheme with second-order accuracy. Subsequently, the pressure-correction PISO algorithm (Pressure-Implicit with Splitting Operators) solves the pressure-velocity linked equations non iteratively. Finally, an Algebraic Multigrid (AMG) method with a Gauss-Seidel relaxation scheme was applied to solve the final linear system of equations.

2.1.6. Mesh Generation

The mesh consists of hexahedral cells and is based on the mesh presented by Sadeghi et al. (2019b). For the mesh independence

study, GC1 and a symmetric vocal fold motion was conducted. Starting with the base mesh (MB) with 2.9 million cells, three more meshes (M1-M3) with a decreasing number of cells were generated, see **Supplementary Table 1**. The limit for the mesh coarsening was set by the Taylor micro-scale $\lambda_T = 0.085\text{mm}$ according to Mihaescu et al. (2010). **Figure 5A**) shows the flow rate for one oscillation cycle. M1-M3 produced a similar trend and the mean relative deviation to MB ranges between -1.3% and $+2.6\%$, see **Supplementary Table 1**. Whereas M3 shows the best accordance with MB in the cycle range 1.4 to 1.8, M1 and M2 deviate from the trend of MB. **Figure 5B** shows an instantaneous pressure evolution at point P1 with a good agreement of meshes M1-M3 in comparison with mesh MB. Small deviations at the beginning and the end of the cycle are visible, which are the result of different instantaneous turbulent fluctuations at point P1 (Sadeghi et al., 2019b), see **Figure 5B**. Summarizing, M3 with the lowest number of cells shows good agreement with the base mesh MB. The resulting mesh M3 is assembled of 1.3 million cells with a basic cell size of 0.68 mm, see **Supplementary Table 1**.

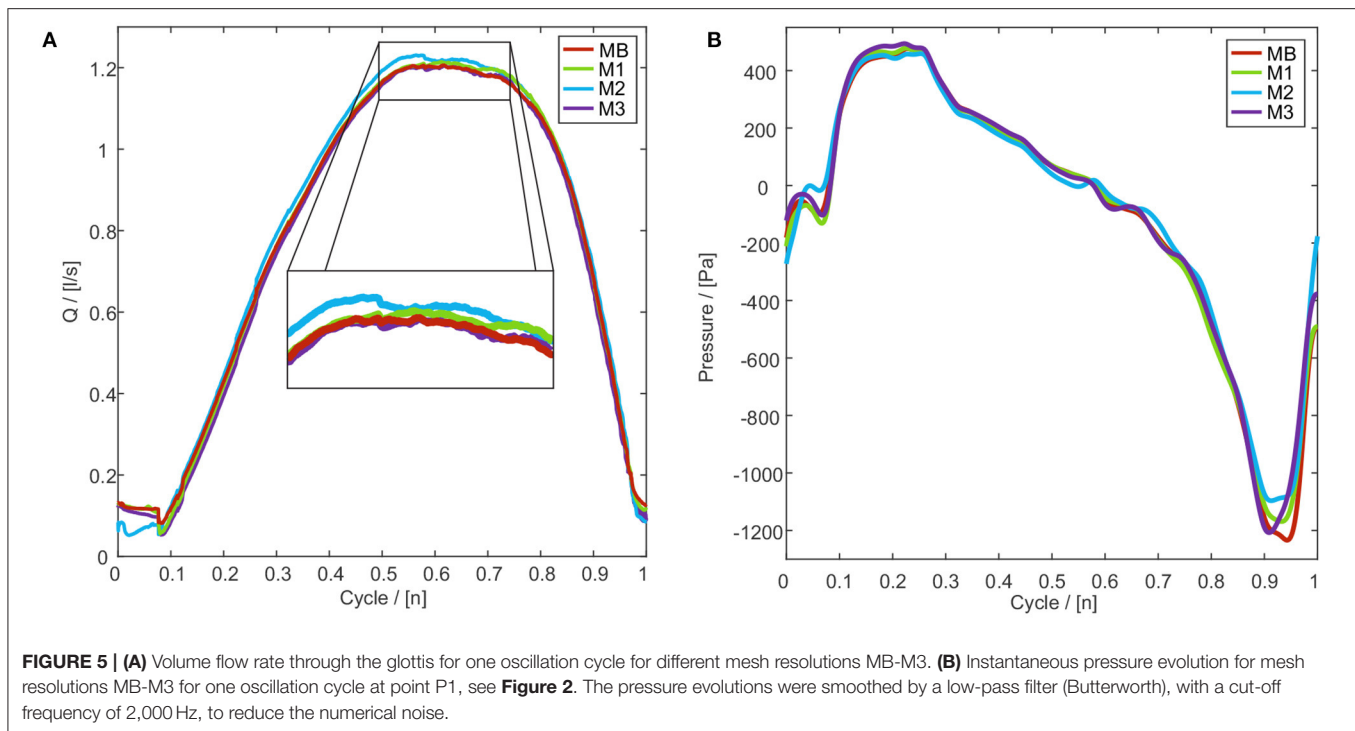
The near-wall flow is modeled by the all- y^+ model of Star-CCM+ that can handle fine and coarse meshes (Reichardt, 1951). The first cell layers on the vocal fold walls have a $y^+ = 1$. The time step size is set to $1.36 \cdot 10^{-6}\text{s}$, and the corresponding mean CFL number is 3.5 that is appropriate for implicit solvers (Anderson, 1995; Hirsch, 2007). *simVoice* uses the overset mesh approach of STAR-CCM+ to realize the vocal fold motion. This chimera method combines a fixed Eulerian background mesh with an Arbitrary Lagrangian-Eulerian (ALE) overlapping mesh (Hadzic, 2005). In *simVoice*, the mesh around both vocal folds represents the overlapping or overset mesh. Consequently, the total number of cells changes over time and depends on the GC type and the distance between the vocal folds during the oscillation.

2.2. *simVoice*—CAA Model

2.2.1. Geometry Dimensions

The acoustic model of *simVoice* has been introduced by Schoder et al. (2020). According to the hybrid aeroacoustic approach, the acoustic domain captures the CFD domain assembled by the larynx and the vocal tract, where the acoustic sources occur. This region is coupled to a propagation domain in which the microphone points Mic1 and Mic2 are located, see **Figure 2B**. These points are positioned on the centerline of the vocal tract at a distance of 5 cm and 8 cm from the vocal tract exit (mouth). Additionally, perfectly matched layers (PML) surround the propagation domain to ensure free field radiation (Kaltenbacher, 2015). Owing to the plane wave approximation, we use an absorbing boundary condition (ABC) at the inlet that requires less computing power compared to PML (Kaltenbacher, 2015). Furthermore, all solid walls are modeled as acoustically hard.

To preserve mesh flexibility and element quality, the acoustic computation grid is composed of two conforming meshes linked via a non-conforming Nitsche-type mortar interface. The mesh of the larynx and the vocal tract was generated for each GC type separately, representing the geometry of the maximum VF opening. It consists of tetrahedral finite elements with a maximum cell size of 5.7 mm. In contrast, the mesh in the



propagation domain is the same for all GC types and has hexahedral elements with a cell size of about 10.9 mm.

2.2.2. Numerical Methods

The aeroacoustic sound generation and acoustic wave propagation is described by the perturbed convective wave equation (PCWE) (Kaltenbacher et al., 2016), which is solved via the finite element solver CFS++ (Schoder et al., 2020). To compute the acoustic source term for the PCWE, the incompressible pressure field from the CFD is transferred onto the CAA mesh by a conservative interpolation scheme based on a cut cell algorithm (Schoder et al., 2019, 2020). The acoustic source term is then computed on the CAA grid as the partial time derivative of the incompressible pressure. We modeled a one-way coupling from the flow to the acoustic sources which was found to be valid for normal voice production (Schoder et al., 2020). A back-coupling effect from the acoustics to the flow field was not considered.

2.3. *simVoice*—Data Acquisition and Analysis

A total of 20 oscillation cycles of the vocal folds were simulated. In a first step, the *simVoice* CFD simulations were executed for 10 oscillation cycles to produce a fully developed flow field. After these 10 initializing oscillations, another 10 oscillation cycles were simulated to provide valid data for the analysis. As shown by **Supplementary Figure 1** the model has achieved repeatable periodic oscillations with the flow field fully converged. The mean cyclic pressure at P1 fluctuates in the range of -7.1 and 9.1% and for P2 in the range of -9.1 and 6.5% , see **Supplementary Figure 1A**). These small fluctuations

highly depend on the turbulent characteristic and the small cycle-to-cycle changes of the fluid flow in the supraglottal region (Kniesburges et al., 2016). The mean volume flow \bar{Q} of the 10 initial oscillations is nearly constant and fluctuates in the range of -0.4 and 1.2% , see **Supplementary Figure 1B**). For the analysis, the complete 3D pressure and velocity fields were exported at every 10th time-step. These flow field data are then imported into CFS++ to determine the acoustic sources and to run the simulation of sound propagation. Finally, the acoustic signals at the two microphone positions were used. The sound pressure level (SPL) was calculated at a reference sound pressure of $p_0 = 20 \mu\text{Pa}$ using a Matlab (Mathworks, USA) routine. Therefore, the acoustic potential of Mic.2, see **Figure 2B**, was extrapolated to a distance of 20 cm far from the vocal tract outlet to match the distance of *ex vivo* studies (Birk et al., 2016, 2017b). The Vocal Efficiency (VE) is calculated as proposed by Riede et al. (2019) and Titze (1992):

$$\text{VE} = \frac{P_r}{P_a} = \frac{4 \cdot \pi \cdot R^2 \cdot 10^{\frac{\text{SPL}-120}{10}}}{P_{\text{sub}} \cdot \bar{Q}} \quad (2)$$

where P_r is the radiated acoustic power, P_a is the aerodynamic power, R is the distance of the microphone to the opening of the vocal tract, P_{sub} is the subglottal pressure, and \bar{Q} is the mean volume flow through the glottis. Additionally, the computed acoustic pressures were analyzed by the in-house Glottis Analysis Tool (GAT) for obtaining the Cepstral Peak Prominence (CPP) (Hillenbrand et al., 1994). The CPP is a spectra-based, well-established and objective measure to judge for perceived breathiness or vocal fatigue (Hillenbrand et al., 1994; Hillenbrand and Houde, 1996; Brinca et al., 2014;

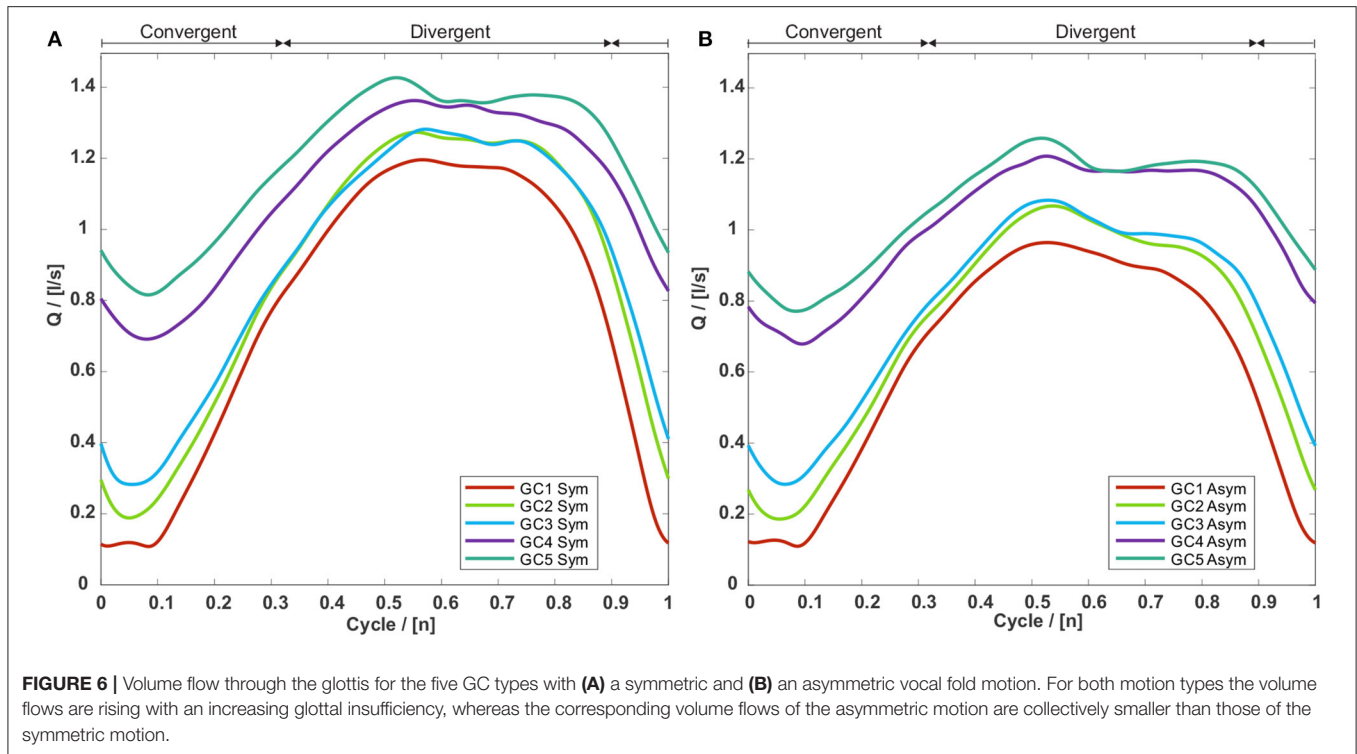


FIGURE 6 | Volume flow through the glottis for the five GC types with (A) a symmetric and (B) an asymmetric vocal fold motion. For both motion types the volume flows are rising with an increasing glottal insufficiency, whereas the corresponding volume flows of the asymmetric motion are collectively smaller than those of the symmetric motion.

Samlan et al., 2014; Samlan and Story, 2017; Patel et al., 2018; Mahalingam et al., 2020; Murton et al., 2020) and has proven to be a more reliable measure of dysphonia than time-based measures (Heman-Ackah et al., 2003). The exact computation procedure is shown in Birk et al. (2016). The CFD data are evaluated concerning the volume flow through the glottis, the glottis resistance as proposed by van den Berg et al. (1957), and the energy transfer between the airflow and the vocal folds tissue. The energy transfer is defined by the work performed by the aerodynamic forces on the moving VFs according to Thomson et al. (2005).

3. RESULTS

3.1. Aerodynamic Characteristics

3.1.1. Volume Flow

The minimum, maximum, and mean volume flow through the glottis consequently increases with an increasing glottal insufficiency from GC1 to GC5 for symmetric and asymmetric vocal fold motions as shown in **Figure 6** and **Table 2**. The flow rate decrease comparing symmetric and asymmetric motion amounts between 9.0% (GC4) and 18.2% (GC1) as displayed in **Table 2**.

3.1.2. Glottis Resistance

The flow resistance across the glottal duct R_{Glottis} (Kniesburges et al., 2017) decreases with an increasing glottal insufficiency. The reason for this decrease in R_{Glottis} is the rising flow rate \bar{Q} , while the P_{sub} remains constant. The direct comparison of R_{Glottis} between symmetric and asymmetric vocal fold motion yielded a

TABLE 2 | Mean volume flow through the glottis \bar{Q} , the glottis resistance R_{Glottis} , and the net energy W_{net} of all GC types.

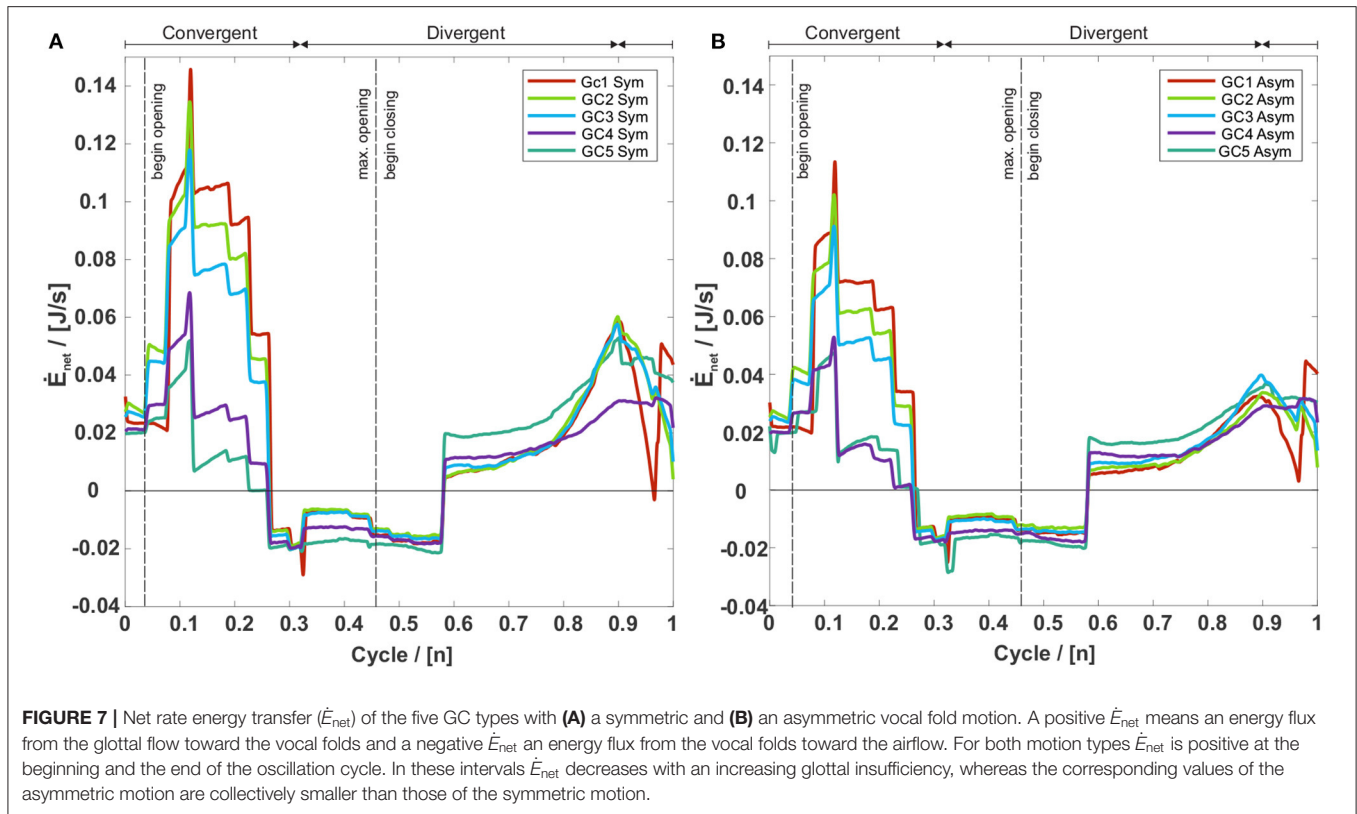
Parameter	GC1	GC2	GC3	GC4	GC5
\bar{Q}^{sym} in [$\frac{\text{l}}{\text{s}}$]	0.77	0.88	0.91	1.11	1.20
\bar{Q}^{asym} in [$\frac{\text{l}}{\text{s}}$]	0.63	0.73	0.78	1.01	1.06
rel.Dev.	-18.2%	-17.0%	-14.3%	-9.0%	-11.7%
$R_{\text{Glottis}}^{\text{sym}}$ in [$\frac{\text{Pa}\cdot\text{s}}{\text{m}^3}$]	1168.9	1044.3	1003.2	845.6	915.0
$R_{\text{Glottis}}^{\text{asym}}$ in [$\frac{\text{Pa}\cdot\text{s}}{\text{m}^3}$]	1397.3	1262.0	1183.5	902.4	1032.3
rel.Dev.	19.5%	20.8%	18.0%	6.7%	12.8%
$W_{\text{net}}^{\text{sym}}$ in [μJ]	165.4	167.1	148.7	73.1	79.1
$W_{\text{net}}^{\text{asym}}$ in [μJ]	114.8	113.1	105.2	54.1	65.2
rel.Dev.	-30.6%	-32.3%	-29.3%	-26.0%	-18.0%

Relative deviation (rel.Dev.) refers to deviation of asymmetric to symmetric motion values. \bar{Q} increases while R_{Glottis} and W_{net} decrease with increasing glottal insufficiency. However, in contrast to R_{Glottis} , W_{net} decreases for asymmetric motion owing to the smaller total amplitude of the glottis oscillation.

larger resistance for the asymmetric motion because \bar{Q} is reduced owing to the smaller glottal gap, see **Table 2**.

3.1.3. Energy Transfer

As proposed by Sadeghi et al. (2019a), the total transferred work (W_{net}) during one oscillation cycle is calculated, see **Table 2**. For both motion types, the total net work during an oscillation cycle is positive, being typical for vocal fold oscillations during phonation (Thomson et al., 2005; Luo et al., 2009). Furthermore,



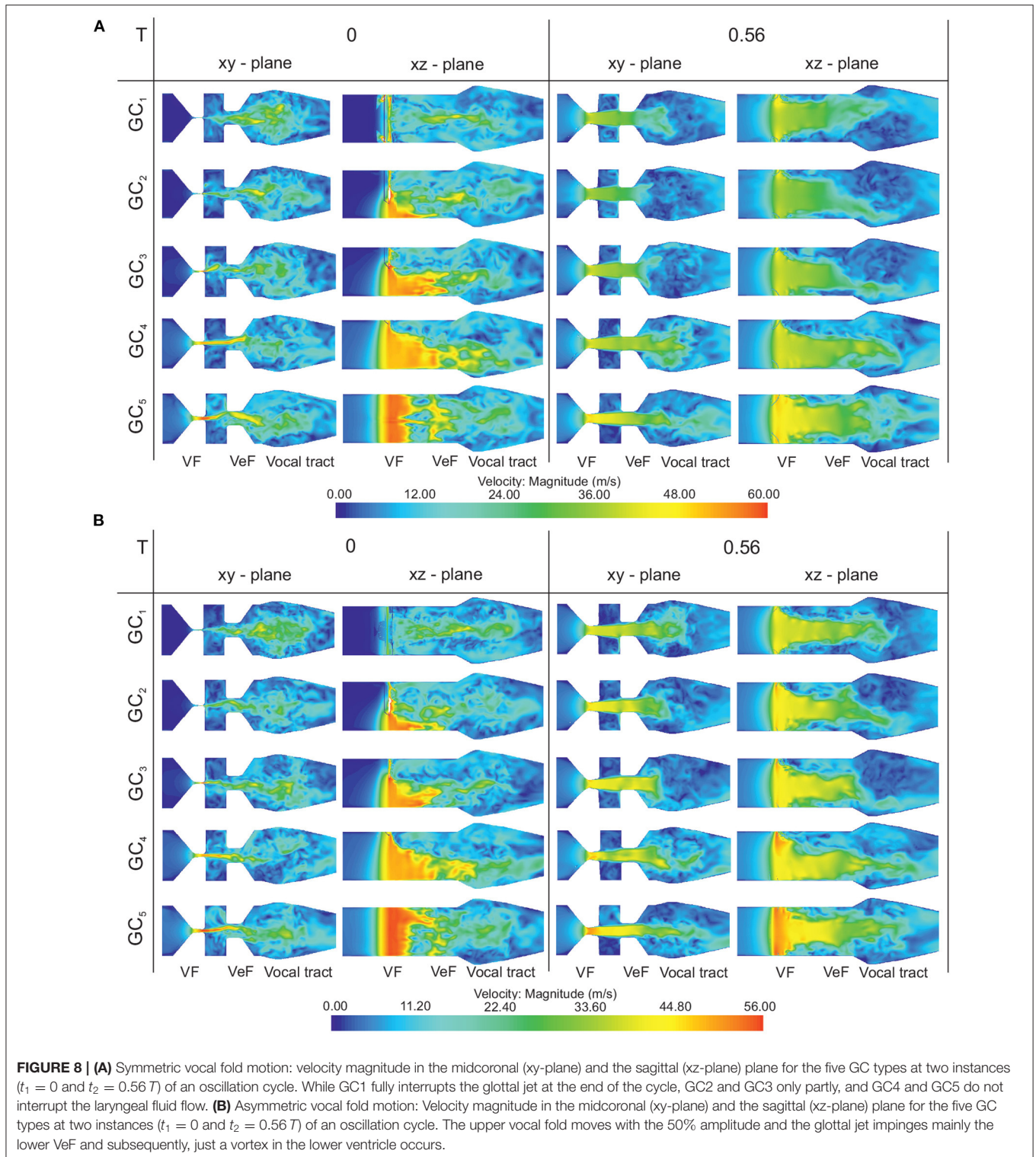
W_{net} decreases with an increasing glottal insufficiency. **Table 2** shows that W_{net} decreases by 55.8% (symmetric) and 52.9% (asymmetric) from GC1 to GC5 whereas the maximum deviation comparing symmetric and asymmetric motion occurs for GC2 with 32.3%. However, in contrast to $R_{Glottis}$, W_{net} decreases for asymmetric motion owing to the smaller total amplitude of the glottis oscillation. Overall, our data shows that a partially closed glottis (GC2 and GC3) in combination with an asymmetric motion produces a higher W_{net} than a contact-free symmetric oscillation, see **Table 2**.

According to Sadeghi et al. (2019a), the time derivative of the work constitutes the net energy transfer rate \dot{E}_{net} between fluid and tissue. It is shown in **Figure 7** for both symmetric and asymmetric vocal fold motions. A positive \dot{E}_{net} corresponds to an energy flux from the laryngeal flow into the tissue, i.e., the flow deforms the vocal folds (Sadeghi et al., 2019a). During the opening, until $0.25 T$, \dot{E}_{net} is positive, which indicates the tissue deformation by the laryngeal flow. Between $0.25 T$ to $0.58 T$, the glottis width reaches its maximum, producing a negative \dot{E}_{net} , resulting from the tissue's resistance to deform further (Sadeghi et al., 2019a). After the flow is fully accelerated, the aerodynamic pressure between the vocal folds is minimal, which initiates the glottis's closing motion. The VFs move toward each other, starting at $0.58 T$, and again a positive \dot{E}_{net} arises. Although the motion of the vocal folds is prescribed in this model, Luo et al. (2009) show a similar energy transfer rate during a cycle of flow-induced VF oscillations. For clarity, we want to mention that the discrete changes in the energy transfer plots occur due to

the frame rate of 4,000 fps of the camera, which was used to record the oscillations of the synthetic vocal folds (Kniesburges et al., 2013). Based on this recording the motion of the vocal folds was modeled without further smoothing and therefore discrete changes in the velocity subsequently occur at multiples of 0.25 ms. **Figure 7** further shows that the positive \dot{E}_{net} during the opening and closing phases decreases with an increasing glottal insufficiency. Furthermore, in the opening and closing phase, \dot{E}_{net} is lower for the asymmetric motion, whereas it is equal for both motion types during the phase of significant tissue resistance ($0.25 T - 0.58 T$).

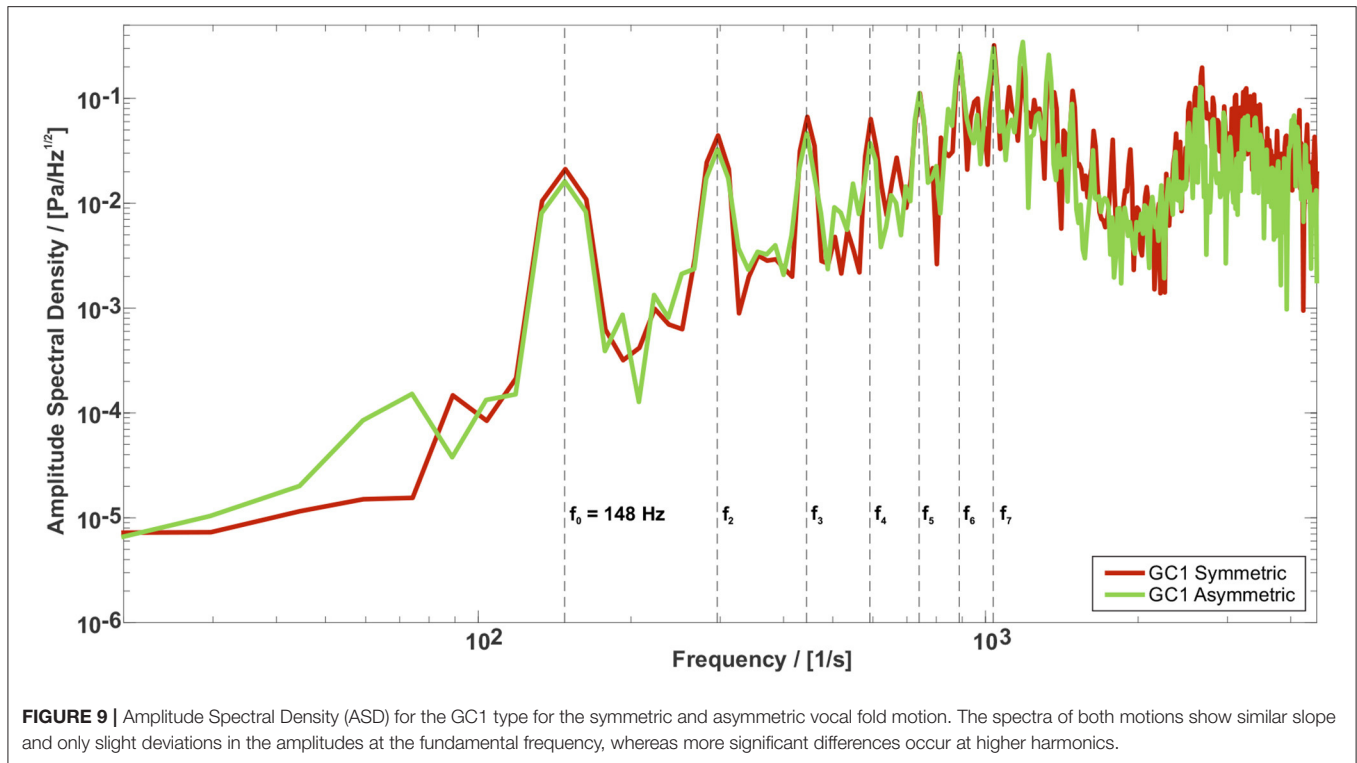
3.1.4. Flow Field Structure

Figure 8 shows the supraglottal flow field at two time instances ($t_1 = 0$ and $t_2 = 0.56 T$) during the oscillation cycle for the symmetric and the asymmetric vocal fold motion. For all GC types, a long jet expands into the supraglottal region. While GC1 fully interrupts this glottal jet at the end of the cycle, GC2 and GC3 only partly interrupt the laryngeal fluid flow at the anterior section of the glottis. For GC4 and GC5, the vocal folds remain open along the entire glottis length during the oscillation cycle, see **Supplementary Videos 3, 4**. This absent interruption of the glottal jet is often related to an aspirated voice signal characterized by lower tonal sound components (Fritzen et al., 1986; Bhatt and Verma, 2014; Kniesburges et al., 2020). As reported by Sadeghi et al. (2018), the VFs have a stabilizing influence on the glottal jet. Therefore, no jet deflection in the medial-lateral



directions (**Figure 8** in the xy-plane) can be observed, see **Supplementary Videos 5, 6**. However, the glottal opening shape has a strong influence on the posterior-anterior jet shape (**Figure 8** in the xz-plane), see also **Supplementary Videos 7, 8**.

As similarly reported by Zörner et al. (2016), triangular glottal orifices deflect the jet toward the larger glottal opening that occurs for GC2 and GC3 at the posterior end of the glottis.



For the symmetric vocal fold motion, the glottal jet impinges both VeF during the oscillation cycle and vortices arise in both ventricles. For the asymmetric case, the glottal jet impinges mainly the lower VeF and subsequently, just a vortex in the lower ventricle occurs, see **Figure 8B** for $t_2 = 0.56 T$ in the xy -plane. Furthermore, the maximum glottal velocity is higher for the symmetric vocal fold motion than for the asymmetric vocal fold motion due to the larger flow rate in the symmetric cases, see color bars in **Figure 8**.

3.2. Quality of Acoustic Voice Signal

3.2.1. Spectral Analysis and Formant Frequencies

Figure 9 shows the amplitude spectral density (ASD) of the sound signals for GC1 and both symmetric and asymmetric vocal folds motions measured at the Mic.1 position, see **Figure 2B**. Both spectra exhibit the main peak at the oscillation frequency of the vocal folds $f_0 = 148 \text{ Hz}$, followed by their harmonics. Comparing the spectra of all GC types shows similar slope and only slight deviations in the amplitudes at the fundamental frequency, whereas more significant differences at the higher harmonics occur, see **Supplementary Figures 2, 3**. Regarding the motion type of the vocal folds, the harmonic tones are more pronounced for the symmetric vocal fold motion, especially in the frequency range between 1,000 and 2,000 Hz. This variance in the acoustic spectra of the radiated sound was also found by Zörner et al. (2016) although the velocity fields of the five GC types are considerably different.

A modal analysis of the vocal tract shows that the first two formants $F_1 = 1,020 \text{ Hz}$ and $F_2 = 1,350 \text{ Hz}$, see transfer

function of /a/ vocal tract in **Supplementary Figure S4**, are well-positioned within the region of the /a/ vowel of the formant chart of Peterson and Barney (1952), shown in **Figure 10**.

3.2.2. Sound Pressure Level (SPL) and Vocal Efficiency (VE)

Figure 11A presents the SPL for all GC types. SPL significantly decreases with an increasing glottal insufficiency: For the symmetric motion type from 91.8 dB for GC1 to 82.4 and 84.2 dB for GC4 and GC5 representing a loss of 10.2 and 8.3%. For the asymmetric motion type, a decrease of about 4.5% for GC2 and GC3, 1.9% for GC4, and 4.9% for GC5, was found compared to SPL = 89.8 dB for GC1. The comparison between both motion types shows only minor differences. A maximum deviation of 6.4% for a higher SPL at the asymmetric motion occurs at GC4. **Figure 11B** shows the VE of all GC types. As mentioned before, the VE is the ratio of radiated acoustic power to aerodynamic power, see Equation (1). According to the SPL, the VE decreases for both vocal fold motion types (symmetric vs. asymmetric) and an increasing degree of glottal insufficiency (GC1 to GC5). The VE decreases from VE = 0.25% for GC1 to VE = 0.03% for GC5 for the symmetric motion and for the asymmetric motion, VE decreases less, from VE = 0.19% (GC1) to VE = 0.04% (GC5).

3.2.3. Cepstral Peak Prominence (CPP)

The CPP is widely used as a quantitative measure for the periodicity of a signal and thereby has proven to be a reliable indicator for the strength of tonal components and therewith the quality of the human voice (Hillenbrand et al., 1994; Hillenbrand

and Houde, 1996; Birk et al., 2017b). It is shown in **Figure 12** for both motion types. The CPP for the symmetric vocal fold motion starts at 17.1 for GC1 and increases to 17.4 for GC2 and GC3.

Afterwards, the CPP decreases to 16.2 dB for GC4 and further to 14.4 dB for GC5. For the asymmetric vocal fold motion the CPP decreases for an increasing glottal insufficiency from 17.1 dB for GC1 to 12.5 dB for GC5.

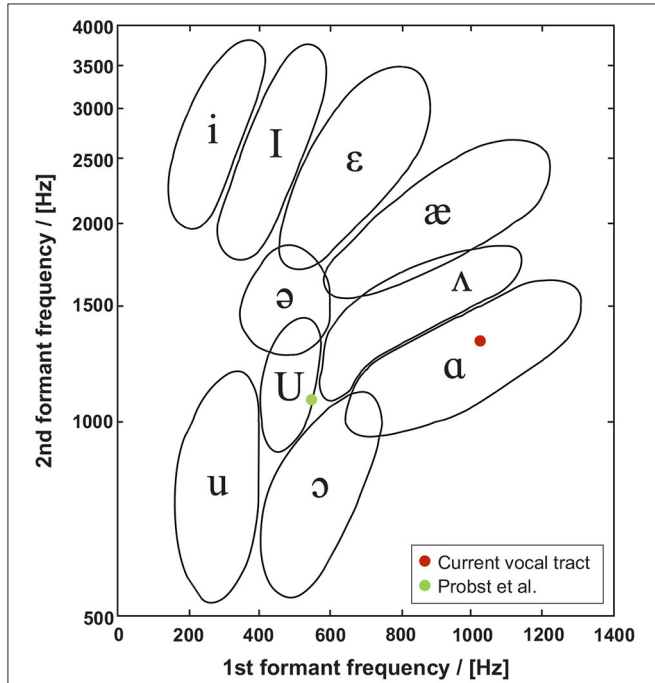


FIGURE 10 | Formant chart as proposed by Peterson and Barney (1952), shows the formant frequencies of the first two formants found in this study and that of Probst et al. (2019). In contrast to Probst et al. (2019), $F1 = 1,020\text{ Hz}$ and $F2 = 1,350\text{ Hz}$ simulated by *simVoice* are well-positioned within the region of the /a/ vowel.

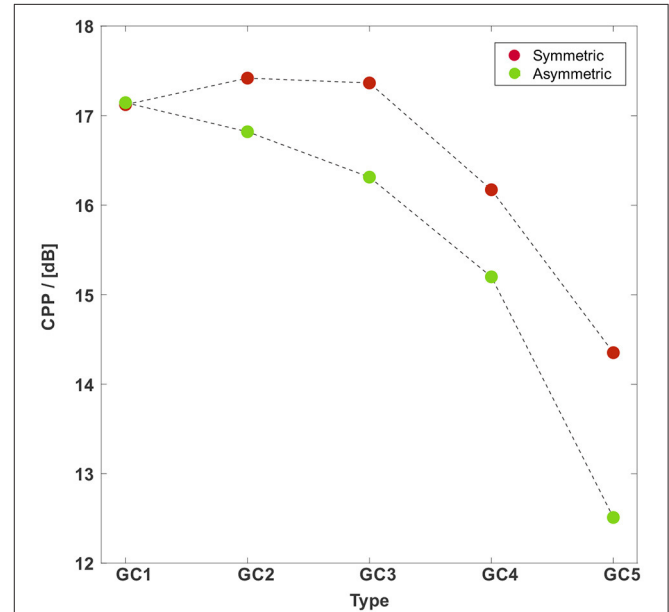


FIGURE 12 | CPP vs. the GC types with a symmetric (red points) and an asymmetric (green points) vocal fold motion. The CPP for the symmetric vocal fold motion almost remains at the same level for GC1 to GC3 followed by a decrease. The CPP for the asymmetric vocal fold motion decreases for an increasing glottal insufficiency. The CPP for the asymmetric motion is collectively smaller than those for the symmetric motion.

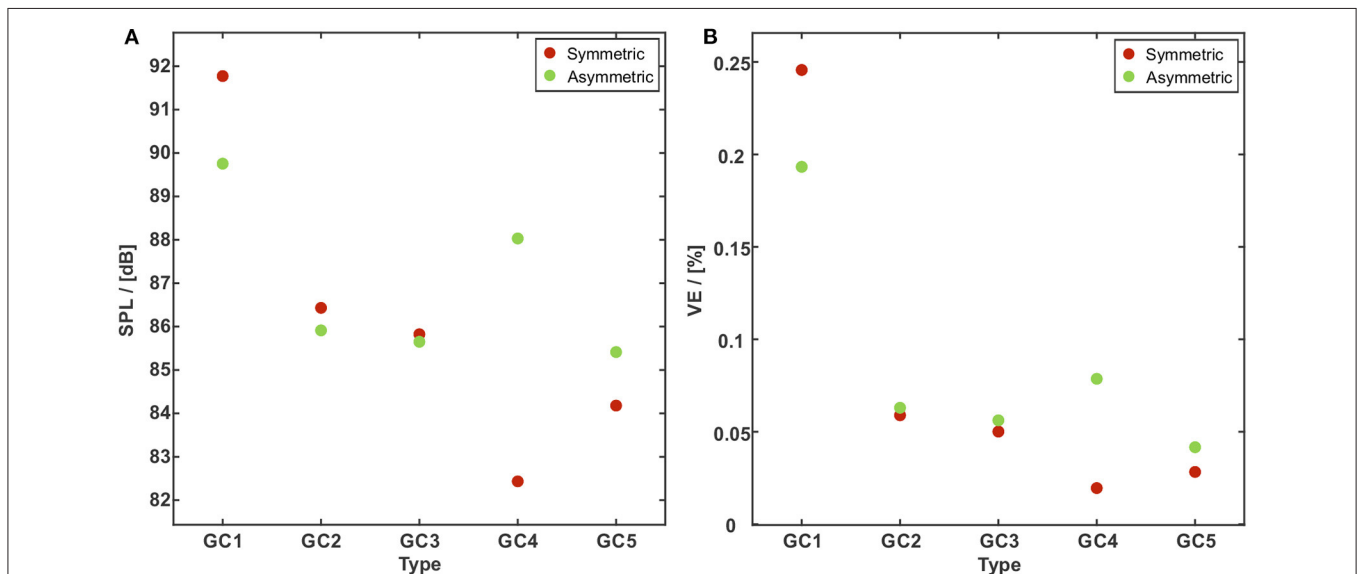


FIGURE 11 | SPL (A) and VE (B) vs. the GC types with a symmetric (red dots) and an asymmetric (green dots) vocal fold motion. The SPL and the VE significantly decrease with an increasing glottal insufficiency. The comparison between both motion types shows significant differences for GC1 and GC4 and only minor differences for GC2, GC3, and GC5.

4. DISCUSSION

4.1. Aerodynamic Characteristics

Our results of the volume flow through the glottis agree with the study by Zañartu et al. (2014) who reported an airflow rise with an increasing posterior gap. As the maximum glottal gap area of an asymmetric type is smaller than its symmetric equivalent, the mean volume flow \bar{Q} is subsequently decreased, see **Table 2**. The left-right asymmetry does not only affect the maximum glottal area as reported by Pickup and Thomson (2009) but also significantly reduces the volume flow through the glottis for a constant inlet pressure in both motion types.

In phonation, the goal is to increase the energy transfer between the glottal airflow and the VFs as a beneficial mechanism to induce the VF oscillation. Kniesburges et al. (2017) interpreted the flow resistance as a measure of energy transfer from the glottal flow to the VFs. Furthermore, Birk et al. (2017b) reported that the energy transfer from the glottal airstream to the vocal folds, as indicated by the glottal resistance, is strongly dependent on glottal insufficiency. In this context, a complete glottis closure during the VFs oscillation produces a large flow resistance R_{Glottis} and in addition a large energy transfer between flow and tissue. Additionally, our data support the findings of Döllinger et al. (2018) which showed that a partially closed glottis (GC2 and GC3) in combination with an asymmetric motion may be still better than a contact-free symmetric oscillation.

In all GC cases, the interaction of the jet with the flow structures in the immediate supraglottal area causes deflection of the tail of the glottal jet. Zhang and Mongeau (2006) reported that this interaction leads to pronounced shear layers between the jet and the resting fluid with large velocity fluctuations.

4.2. Quality of Acoustic Signal

As described above, the vocal tract model is the smoothed version of the staged model developed by Probst et al. (2019). They reported formant frequencies of $F_1 = 550 \text{ Hz}$ and $F_2 = 1,080 \text{ Hz}$, being lower than the formants found here. We assume the shift of the first two formants in this study to higher values is due to the vocal tract smoothing. As reported by Jiang et al. (2017) the location of the formants and a resulting shift significantly depends on the area variation along the tract. Probst et al. (2019) and Jiang et al. (2017) found lower frequencies for the first two formants, but Jiang et al. (2017) used a vocal tract, mimicking a neutral vowel /schwa/ superimposed onto a realistic airway centerline from *in vivo* MRI measurements. Comparing the third formant F_3 of our model with that of Probst et al. (2019) shows a good agreement.

Moreover, the results of SPL show good qualitative agreement with those reported by Thornton et al. (2019) and Döllinger et al. (2018), see **Table 3**. They executed *ex vivo* experiments with rabbit larynxes and three different glottal insufficiency grades (complete glottal closure, partial glottal closure, no contact of vocal folds). They measured the SPL at a distance of 20 cm from the glottis. Furthermore, our SPL is higher than the *in vivo* measurements of Södersten et al. (1995) because the microphone in our model is located 30 cm closer to the vocal folds, nevertheless our SPL values are in the human range

TABLE 3 | SPL in [dB] of Döllinger et al. (2018) and Thornton et al. (2019).

SPL in [dB]	GC1 closed	GC2/GC3 partially closed	GC4 no contact
Döllinger et al., 2018	79.1 ± 6.4	76.1 ± 7.1	69.4 ± 7.5
Thornton et al., 2019	76.7 ± 6.5	76.0 ± 7.6	59.4 ± 7.5

Even though our SPL values are higher they show good qualitative agreement with the trends reported in this study.

TABLE 4 | CPP in [dB] of Birk et al. (2017b), Döllinger et al. (2018), and Thornton et al. (2019).

CPP in [dB]	GC1 closed	GC2 30% partially closed	GC3 60% partially closed	GC4 no contact
Birk et al., 2017b	24.3 ± 5.82	21.8 ± 4.2	16.4 ± 2.82	15.7 ± 1.94
Döllinger et al., 2018	24.0 ± 4.8	22.8 ± 4.8		19.4 ± 4.9
Thornton et al., 2019	17.9 ± 4.3	15.8 ± 6.5		11.0 ± 3.4

Quantitatively, our CPP values are in the range of values reported there.

(Gramming et al., 1988). Our results show that an increasing posterior gap and glottal insufficiency may reduce the SPL as reported by Zañartu et al. (2014).

Tanaka and Gould (1985) found a low VE with a large glottal gap and a high flow rate. Due to the dependency of the radiated acoustic power from the mouth opening and therefore from the vowels (Titze et al., 2016), our results may be just valid for a vowel /a/. Although the basic trend of the VE for the asymmetric motion coincides with that for symmetric motion, the VE is mostly larger (GC2 to GC5) compared to the symmetric motion and is just lower for GC1. Thus, our results agree for GC1 with the study by Oren et al. (2016), who reported a reduction of VE for asymmetric vocal fold motion (the study does not present the degree of glottal insufficiency). We could not identify a discrete effect that produces the outlier in SPL and subsequently in VE for GC4. We assume a cumulative effect that may occur mainly in the higher frequency range of the acoustic signal.

Both effects, an increasing insufficiency, and an asymmetric vocal fold motion potentially reduce the tonal components of the acoustic signal and the voice quality. The same observations have been made in *in vivo* studies executed by Samlan et al. (2014) and Chen et al. (2011). Furthermore, the qualitative trend of CPP was also found in *ex vivo* studies with human (Birk et al., 2017b) and rabbit larynxes (Döllinger et al., 2018; Thornton et al., 2019), as shown in **Table 4**. The high CPP values for GC2 and GC3 for symmetrically oscillating VFs shows, that the acoustic signal is still tonal and physiological for small posterior gaps as often observed in physiological phonation of women and children (Södersten and Lindestad, 1990; Södersten et al., 1995; Inwald et al., 2010; Patel et al., 2012; Kniesburges et al., 2020). Quantitatively, our CPP values are in the range of values reported by Döllinger et al. (2018) and Thornton et al. (2019).

4.3. Limitations of the Study

The vocal fold vibration in this study is prescribed, neglecting the fluid-structure interaction (FSI), which is a common approach to increase the efficiency of the simulations.

5. CONCLUSION

Glottal insufficiency and asymmetric vocal fold oscillations have been investigated using our numerical aeroacoustic model *simVoice*. Aerodynamically, an increasing degree of glottal insufficiency leads to a decrease in flow resistance and a decrease in the energy transfer rate between flow and tissue. This means a reduction of the stimulation of the vocal fold oscillations and subsequently impairs the acoustic signal. Thus, CPP (Hillenbrand and Houde, 1996; Birk et al., 2017b; Döllinger et al., 2018; Thornton et al., 2019), SPL (Döllinger et al., 2018; Thornton et al., 2019), and VE (Tanaka and Gould, 1985) deteriorate for an increasing degree of glottal insufficiency.

All these findings correlate with symptoms of functional voice disorders such as breathiness, hoarseness, and an enhanced effort needed to phonate, commonly called air loss during phonation (Fritzen et al., 1986; Zhang, 2019). However, a glottis insufficiency can also occur in physiological phonation often observed in women and children who have a triangular-shaped opening located in the posterior glottis (Södersten and Lindestad, 1990; Södersten et al., 1995; Inwald et al., 2010; Patel et al., 2012; Kniesburges et al., 2020). Those persons have often a soft and quiet voice as reported by Fritzen et al. (1986) and Bhatt and Verma (2014).

In principle, the same trend of a deterioration for an increasing degree of glottal insufficiency for CPP, SPL and VE can be seen when comparing symmetric and asymmetric motion of the vocal folds: The energy transfer rate and the acoustic parameters decrease for asymmetric motion. However, this trend is not that distinct as for glottal insufficiency (Birk et al., 2017b). Therefore, a left-right asymmetry must not necessarily result in a salient reduction in voice quality, as similarly reported by Zhang et al. (2012).

From our results, we assume that a high degree of glottal insufficiency potentially displays the most severe symptom for a functional voice disorder, which has to be focused on during clinical treatment [e.g., medialization with hyaluronic acid-based materials or thyroplasty (type 1 thyroplasty)]. Thereby, the asymmetry of the motion of the vocal folds seems to have a reduced role in negatively impacting the voice quality compared to the glottal insufficiency. But both symptoms in combination will further reduce the quality of the sound signal.

REFERENCES

Alku, P., Airas, M., Björkner, E., and Sundberg, J. (2006). An amplitude quotient based method to analyze changes in the shape of the glottal pulse in the regulation of vocal intensity. *J. Acoust. Soc. Am.* 120, 1052–1062. doi: 10.1121/1.2211589

Regarding the functionality of *simVoice*, the study shows: (1) *simVoice* can mimic simplified vibration characteristics and glottal geometries, (2) *simVoice* reveals separated and combined effects of aerodynamic and acoustic symptoms of a glottal insufficiency and an asymmetric vocal fold motion, and (3) a current walltime of 10 h/cycle is, with a prospective increase in computing power, very promising for a clinical approach.

Furthermore, CFD data in addition to experimental data are essential to develop, train and validate neural networks as done by Zhang (2020) and Zhang et al. (2020), which will further speed up the computing time of the phonation process and the implementing of numerical models in the clinical environment.

DATA AVAILABILITY STATEMENT

The original contributions presented in the study are included in the article/**supplementary material**, further inquiries can be directed to the corresponding author/s.

AUTHOR CONTRIBUTIONS

MD, MK, and SK conceived the study and contributed to data analysis and interpretation, supervision, and manuscript writing. SF conducted main writing and review editing. SF, BJ, SS, and PM conducted the CFD and CAA simulations, and contributed to data analysis, interpretation and manuscript writing. ME contributed to results interpretation, clinical input, review editing and provided the VT geometry. All authors contributed to the article and approved submitted version.

FUNDING

The authors acknowledge support from the German Research Foundation (DFG) under DO 1247/10-1 (no. 391215328) and the Austrian Research Council (FWF) under no. I 3702.

ACKNOWLEDGMENTS

Furthermore, the authors acknowledge support from the Central Institute for Scientific Computing (ZISC) and computational resources and support provided by the Erlangen Regional Computing Center (RRZE).

SUPPLEMENTARY MATERIAL

The Supplementary Material for this article can be found online at: <https://www.frontiersin.org/articles/10.3389/fphys.2021.616985/full#supplementary-material>

Anderson, J. (1995). *Computational Fluid Dynamics: The Basics with Applications*. New York, NY: McGraw-Hill.

Arnella, M., Dabbaghchian, S., Blandin, R., Guasch, O., Engwall, O., Van Hirtum, A., et al. (2016). Influence of vocal tract geometry simplifications on the numerical simulation of vowel sounds. *J. Acoust. Soc. Am.* 140, 1707–1718. doi: 10.1121/1.4962488

- Aronson, A., and Bless, D. (2009). *Clinical Voice Disorders, 4th Edn.* New York, NY: Thieme.
- Baken, R. J., and Orlikoff, R. F. (2000). *Clinical Measurement of Speech and Voice.* San Diego, CA: Singular.
- Becker, S., Kniesburges, S., Müller, S., Delgado, A., Link, G., Kaltenbacher, M., et al. (2009). Flow-structure-acoustic interaction in a human voice model. *J. Acoust. Soc. Am.* 125, 1351–1361. doi: 10.1121/1.3068444
- Bhatt, J., and Verma, S. (2014). Management of glottal insufficiency. *Otorinolaringologia* 64, 101–107.
- Birk, V., Döllinger, M., Sutor, A., Berry, D. A., Gedeon, D., Traxdorf, M., et al. (2017a). Automated setup for *ex vivo* larynx experiments. *J. Acoust. Soc. Am.* 141, 1349–1359. doi: 10.1121/1.4976085
- Birk, V., Kniesburges, S., Semmler, M., Berry, D. A., Bohr, C., Döllinger, M., et al. (2017b). Influence of glottal closure on the phonatory process in *ex vivo* porcine larynges. *J. Acoust. Soc. Am.* 142, 2197–2207. doi: 10.1121/1.5007952
- Birk, V., Sutor, A., Döllinger, M., Bohr, C., and Kniesburges, S. (2016). Acoustic impact of ventricular folds on phonation studied in *ex vivo* human larynx models. *Acta Acust. Unit. Acust.* 102, 244–256. doi: 10.3813/AAA.918941
- Boessenecker, A., Berry, D. A., Lohscheller, J., Eysholdt, U., and Döllinger, M. (2007). Mucosal wave properties of a human vocal fold. *Acta Acust. Unit. Acust.* 93, 815–823.
- Brinca, L. F., Batista, A. P. F., Tavares, A. I., Gonçalves, I. C., and Moreno, M. L. (2014). Use of cepstral analyses for differentiating normal from dysphonic voices: a comparative study of connected speech versus sustained vowel in European Portuguese female speakers. *J. Voice* 28, 282–286. doi: 10.1016/j.jvoice.2013.10.001
- Chen, G., Kreiman, J., Shue, Y.-L., and Alwan, A. (2011). “Acoustic correlates of glottal gaps,” in *Twelfth Annual Conference of the International Speech Communication Association.* Florence.
- de Oliveira Rosa, M., Pereira, J. C., Grellet, M., and Alwan, A. (2003). A contribution to simulating a three-dimensional larynx model using the finite element method. *J. Acoust. Soc. Am.* 114, 2893–2905. doi: 10.1121/1.1619981
- Döllinger, M., and Berry, D. A. (2006a). Computation of the three-dimensional medial surface dynamics of the vocal folds. *J. Biomech.* 39, 369–374. doi: 10.1016/j.jbiomech.2004.11.026
- Döllinger, M., and Berry, D. A. (2006b). Visualization and quantification of the medial surface dynamics of an excised human vocal fold during phonation. *J. Voice* 20, 401–413. doi: 10.1016/j.jvoice.2005.08.003
- Döllinger, M., Berry, D. A., and Kniesburges, S. (2016). Dynamic vocal fold parameters with changing adduction in *ex-vivo* hemilarynx experiments. *J. Acoust. Soc. Am.* 139, 2372–2385. doi: 10.1121/1.4947044
- Döllinger, M., Dubrovskiy, D., and Patel, R. (2012). Spatiotemporal analysis of vocal fold vibrations between children and adults. *Laryngoscope* 122, 2511–2518. doi: 10.1002/lary.23568
- Döllinger, M., Gröhn, F., Berry, D. A., Eysholdt, U., and Luegmair, G. (2014). Preliminary results on the influence of engineered artificial mucus layer on phonation. *J. Speech Lang. Hear. Res.* 57, 637–647. doi: 10.1044/2014_JSLHR-S-12-0277
- Döllinger, M., Kniesburges, S., Berry, D. A., Birk, V., Wendler, O., Dürr, S., et al. (2018). Investigation of phonatory characteristics using *ex vivo* rabbit larynges. *J. Acoust. Soc. Am.* 144, 142–152. doi: 10.1121/1.5043384
- Döllinger, M., Tayama, N., and Berry, D. A. (2005). Empirical eigenfunctions and medial surface dynamics of a human vocal fold. *Methods Inform. Med.* 44, 384–391. doi: 10.1055/s-0038-1633981
- Echternach, M., Sundberg, J., Baumann, T., Markl, M., and Richter, B. (2011). Vocal tract area functions and formant frequencies in opera tenors’ modal and falsetto registers. *J. Acoust. Soc. Am.* 129, 3955–3963. doi: 10.1121/1.3589249
- Eysholdt, U., Rosanowski, F., and Hoppe, U. (2003). Vocal fold vibration irregularities caused by different types of laryngeal asymmetry. *Eur. Arch. Otorhinolaryngol.* 260, 412–417. doi: 10.1007/s00405-003-0606-y
- Fritzen, B., Hammarberg, B., Gaffin, J., and Karlsson, I. (1986). Breathiness and insufficient vocal fold closure. *Elsevier* 14, 549–553. doi: 10.1016/S0095-4470(19)30705-3
- George, N. A., de Mul, F. F., Qiu, Q., Rakhorst, G., and Schutte, H. K. (2008). Depth-kymography: high-speed calibrated 3D imaging of human vocal fold vibration dynamics. *Phys. Med. Biol.* 53, 2667–2675. doi: 10.1088/0031-9155/53/10/015
- Gramming, P., Sundberg, J., Ternström, S., Leanderson, R., and Perkins, W. H. (1988). Relationship between changes in voice pitch and loudness. *J. Voice* 2, 118–126. doi: 10.1016/S0892-1997(88)80067-5
- Hadzic, H. (2005). *Development and application of a finite volume method for the computation of flows around moving bodies on unstructured, overlapping grids* (Ph.D. thesis). Hamburg: Technische Universität Hamburg.
- Heman-Ackah, Y. D., Heuer, R. J., Michael, D. D., Ostrowski, R., Horman, M., Baroody, M. M., et al. (2003). Cepstral peak prominence: a more reliable measure of dysphonia. *Ann. Otol. Rhinol. Laryngol.* 112, 324–333. doi: 10.1177/000348940311200406
- Hillenbrand, J., Cleveland, R. A., and Erickson, R. L. (1994). Acoustic correlates of breathy vocal quality. *J. Speech Hear. Res.* 37, 769–778. doi: 10.1044/jshr.3704.769
- Hillenbrand, J., and Houde, R. A. (1996). Acoustic correlates of breathy vocal quality: dysphonic voices and continuous speech. *J. Speech Hear. Res.* 39, 311–321. doi: 10.1044/jshr.3902.311
- Hirsch, C. (2007). *Numerical Computation of Internal and External Flows: The Fundamentals of Computational Fluid Dynamics, 2nd edn.* Oxford: Elsevier Ltd.
- Hoffman, M. R., Surender, K., Devine, E. E., and Jiang, J. J. (2012). Classification of glottic insufficiency and tension asymmetry using a multilayer perceptron. *Laryngoscope* 122, 2773–2780. doi: 10.1002/lary.23549
- Holmberg, E. B., Hillman, R. E., and Perkell, J. S. (1988). Glottal airflow and transglottal air pressure measurements for male and female speakers in soft, normal, and loud voice. *J. Acoust. Soc. Am.* 84, 511–529. doi: 10.1121/1.396829
- Hoppe, U., Rosanowski, F., Döllinger, M., Lohscheller, J., Schuster, M., and Eysholdt, U. (2003). Glissando: laryngeal motorics and acoustics. *J. Voice* 17, 370–376. doi: 10.1067/S0892-1997(03)00019-5
- Inwald, E., Döllinger, M., Schuster, M., Eysholdt, U., and Bohr, C. (2010). Multiparametric analysis of vocal fold vibrations in healthy and disordered voices in high-speed imaging. *J. Voice* 25, 576–590. doi: 10.1016/j.jvoice.2010.04.004
- Jiang, W., Zheng, X., and Xue, Q. (2017). Computational modeling of fluid-structure-acoustics interaction during voice production. *Front. Bioeng. Biotechnol.* 5:7. doi: 10.3389/fbioe.2017.00007
- Jo, Y., Ra, H., Moon, Y. J., and Döllinger, M. (2016). Three-dimensional computation of flow and sound for human hemilarynx. *Comput. Fluids* 134–135:41–50. doi: 10.1016/j.compfluid.2016.04.029
- Kaltenbacher, M. (2015). *Numerical Simulation of Mechatronic Sensors and Actuators: Finite Elements for Computational Multiphysics, 3rd Edn.* Berlin: Springer.
- Kaltenbacher, M., Hüppe, A., Grabinger, J., and Wohlmuth, B. (2016). Modeling and finite element formulation for acoustic problems including rotating domains. *AIAA J.* 54, 3768–3777. doi: 10.2514/1.J054890
- Kaltenbacher, M., Zörner, S., and Hüppe, A. (2014). On the importance of strong fluid-solid coupling with application to human phonation. *Prog. Comput. Fluid Dyn.* 14, 2–13. doi: 10.1504/PCFD.2014.059195
- Kirmse, C., Triep, M., Brücker, C., Döllinger, M., and Stingl, M. (2010). Experimental flow study of modeled regular and irregular glottal closure types. *Logoped. Phoniater. Vocol.* 35, 45–50. doi: 10.3109/14015431003667652
- Kniesburges, S. (2014). *Fluid-structure-acoustic interaction during phonation in a synthetic larynx model* (Ph.D. thesis). Aachen: Shaker Verlag.
- Kniesburges, S., Birk, V., Lodermeier, A., Schützenberger, A., Bohr, C., and Becker, S. (2017). Effect of the ventricular folds in a synthetic larynx model. *J. Biomech.* 55, 128–133. doi: 10.1016/j.jbiomech.2017.02.021
- Kniesburges, S., Hesselmann, C., Becker, S., Schlücker, E., and Döllinger, M. (2013). Influence of vortical flow structures on the glottal jet location in the supraglottal region. *J. Voice* 27, 531–544. doi: 10.1016/j.jvoice.2013.04.005
- Kniesburges, S., Lodermeier, A., Becker, S., Traxdorf, M., and Döllinger, M. (2016). The mechanisms of subharmonic tone generation in a synthetic larynx model. *J. Acoust. Soc. Am.* 139, 3182–3192. doi: 10.1121/1.4954264
- Kniesburges, S., Lodermeier, A., Semmler, M., Schulz, Y. K., Schützenberger, A., and Becker, S. (2020). Analysis of the tonal sound generation during phonation with and without glottis closure. *J. Acoust. Soc. Am.* 147:3285. doi: 10.1121/10.0001184
- Kniesburges, S., Thomson, S. L., Barney, A., Triep, M., Petr, Š., Horáček, J., et al. (2011). *In vitro* experimental investigation of voice production. *Curr. Bioinform.* 6, 305–322. doi: 10.2174/157489311796904637

- Lagier, A., Guenoun, D., Legou, T., Espesser, R., Giovanni, A., and Champsaur, P. (2017). Control of the glottal configuration in ex vivo human models: quantitative anatomy for clinical and experimental practices. *Surg. Radiol. Anat.* 39, 257–262. doi: 10.1007/s00276-016-1738-2
- Larsson, H., and Hertegård, S. (2004). Calibration of high-speed imaging by laser triangulation. *Logoped. Phoniater. Vocol.* 29, 154–161. doi: 10.1080/14015430410024353
- Link, G., Kaltenbacher, M., Breuer, M., and Döllinger, M. (2009). A 2D finite-element scheme for fluid-solid-acoustic interactions and its application to human phonation. *Comput. Methods Appl. Mech. Eng.* 198, 3321–3334. doi: 10.1016/j.cma.2009.06.009
- Lodermeier, A., Becker, S., Döllinger, M., and Kniesburges, S. (2015). Phase-locked flow field analysis in a synthetic human larynx model. *Exp. Fluids* 56, 1–13. doi: 10.1007/s00348-015-1942-6
- Lodermeier, A., Tautz, M., Becker, S., Döllinger, M., Birk, V., and Kniesburges, S. (2018). Aeroacoustic analysis of the human phonation process based on a hybrid acoustic PIV approach. *Exp. Fluids* 59, 1–15. doi: 10.1007/s00348-017-2469-9
- Luo, H., Mittal, R., and Bielamowicz, S. A. (2009). Analysis of flow-structure interaction in the larynx during phonation using an immersed-boundary method. *J. Acoust. Soc. Am.* 126, 816–824. doi: 10.1121/1.3158942
- Luo, H., Mittal, R., Zheng, X., Bielamowicz, S. A., Walsh, R. J., and Hahn, J. K. (2008). An immersed-boundary method for flow-structure interaction in biological systems with application to phonation. *J. Comput. Phys.* 227, 9303–9332. doi: 10.1016/j.jcp.2008.05.001
- Mahalingam, S., Boominathan, P., Arunachalam, R., Venkatesh, L., and Srinivas, S. (2020). Cepstral measures to analyze vocal fatigue in individuals with hyperfunctional voice disorder. *J. Voice*. doi: 10.1016/j.jvoice.2020.02.007. [Epub ahead of print].
- Mendelsohn, A. H., Zhang, Z., Luegmair, G., Orestes, M., and Berke, G. S. (2015). Preliminary study of the open quotient in an ex vivo perfused human larynx. *JAMA Otolaryngol.* 141, 751–756. doi: 10.1001/jamaoto.2015.1249
- Mihaescu, M., Khosla, S. M., Murugappan, S., and Gutmark, E. J. (2010). Unsteady laryngeal airflow simulations of the intra-glottal vortical structures. *J. Acoust. Soc. Am.* 127, 435–444. doi: 10.1121/1.3271276
- Motie-Shirazi, M., Zaňartu, M., Peterson, S. D., Mehta, D. D., Kobler, J. B., Hillman, R. E., et al. (2019). Toward development of a vocal fold contact pressure probe: sensor characterization and validation using synthetic vocal fold models. *Appl. Sci.* 9:3002. doi: 10.3390/app9153002
- Murray, P. R., and Thomson, S. L. (2012). Vibratory responses of synthetic, self-oscillating vocal fold models. *J. Acoust. Soc. Am.* 132, 3428–3438. doi: 10.1121/1.4754551
- Murton, O., Hillman, R., and Mehta, D. (2020). Cepstral peak prominence values for clinical voice evaluation. *Am. J. Speech Lang. Pathol.* 29, 1596–1607. doi: 10.1044/2020_AJSLP-20-00001
- Nicoud, F., and Ducros, F. (1999). Subgrid-scale stress modelling based on the square of the velocity gradient tensor. *Flow Turbul. Combust.* 62, 183–200. doi: 10.1023/A:1009995426001
- Oren, L., Khosla, S., and Gutmark, E. (2016). Effect of vocal fold asymmetries on glottal flow. *Laryngoscope* 126, 2534–2538. doi: 10.1002/lary.25948
- Park, J. B., and Mongeau, L. (2008). Experimental investigation of the influence of a posterior gap on glottal flow and sound. *J. Acoust. Soc. Am.* 124, 1171–1179. doi: 10.1121/1.2945116
- Patel, R. R., Awan, S. N., Barkmeier-Kraemer, J., Courey, M., Deliyiski, D., Eadie, T., et al. (2018). Recommended protocols for instrumental assessment of voice: American speech-language-hearing association expert panel to develop a protocol for instrumental assessment of vocal function. *Am. J. Speech Lang. Pathol.* 27, 887–905. doi: 10.1044/2018_AJSLP-17-0009
- Patel, R. R., Dixon, A., Richmond, A. M., and Donohue, K. D. (2012). Pediatric high speed digital imaging of vocal fold vibration: a normative pilot study of glottal closure and phase closure characteristics. *Int. J. Pediatr. Otorhinolaryngol.* 76, 954–959. doi: 10.1016/j.ijporl.2012.03.004
- Peterson, G. E., and Barney, H. L. (1952). Control methods used in a study of the vowels. *J. Acoust. Soc. Am.* 24, 175–184. doi: 10.1121/1.1906875
- Pickup, B. A., and Thomson, S. L. (2009). Influence of asymmetric stiffness on the structural and aerodynamic response of synthetic vocal fold models. *J. Biomech.* 42, 2219–2225. doi: 10.1016/j.jbiomech.2009.06.039
- Probst, J., Lodermeier, A., Fattoum, S., Becker, S., Echternach, M., Richter, B., et al. (2019). Acoustic and aerodynamic coupling during phonation in MRI-based vocal tract replicas. *Appl. Sci.* 9:3562. doi: 10.3390/app9173562
- Rammage, L. A., Peppard, R. C., and Bless, D. M. (1992). Aerodynamic, laryngoscopic, and perceptual-acoustic characteristics in dysphonic females with posterior glottal chinks: a retrospective study. *J. Voice* 6, 64–78. doi: 10.1016/S0892-1997(05)80010-4
- Reichardt, H. (1951). Vollständige Darstellung der turbulenten Geschwindigkeitsverteilung in glatten Leitungen. *Zeitschrift für Angewandte Mathematik und Mechanik* 31, 208–219. doi: 10.1002/zamm.19510310704
- Riede, T., Thomson, S. L., Titze, I. R., and Goller, F. (2019). The evolution of the syrinx: An acoustic theory. *PLoS Biol.* 17:e2006507. doi: 10.1371/journal.pbio.2006507
- Rogers, D. J., Setlur, J., Raol, N., Maurer, R., and Hartnick, C. J. (2014). Evaluation of true vocal fold growth as a function of age. *Otolaryngol. Head Neck Surg.* 151, 681–686. doi: 10.1177/0194599814547489
- Romero, R. G., Colton, M. B., and Thomson, S. L. (2020). 3D-printed synthetic vocal fold models. *Journal of Voice*. doi: 10.1016/j.jvoice.2020.01.030. [Epub ahead of print].
- Ruben, R. J. (2000). Redefining the survival of the fittest: communication disorders in the 21st century. *Laryngoscope* 110, 241–241. doi: 10.1097/00005537-200002010-00010
- Sadeghi, H. (2019). *Large eddy simulations of phonatory aerodynamics in a 3D-FVM larynx model* (Ph.D. thesis). Friedrich-Alexander University Erlangen, Erlangen, Germany.
- Sadeghi, H., Döllinger, M., Kaltenbacher, M., and Kniesburges, S. (2019a). Aerodynamic impact of the ventricular folds in computational larynx models. *J. Acoust. Soc. Am.* 145, 2376–2387. doi: 10.1121/1.5098775
- Sadeghi, H., Kniesburges, S., Falk, S., Kaltenbacher, M., Schützenberger, A., and Döllinger, M. (2019b). Towards a clinically applicable computational larynx model. *Appl. Sci.* 9:2288. doi: 10.3390/app9112288
- Sadeghi, H., Kniesburges, S., Kaltenbacher, M., Schützenberger, A., and Döllinger, M. (2018). Computational models of laryngeal aerodynamics: potentials and numerical costs. *J. Voice* 33, 385–400. doi: 10.1016/j.jvoice.2018.01.001
- Samlan, R. A., and Story, B. H. (2017). Influence of left-right asymmetries on voice quality in simulated paramedian vocal fold paralysis. *J. Speech Lang. Hear. Res.* 60, 306–321. doi: 10.1044/2016_JSLHR-S-16-0076
- Samlan, R. A., Story, B. H., Lotto, A. J., and Bunton, K. (2014). Acoustic and perceptual effects of left-right laryngeal asymmetries based on computational modeling. *J. Speech Lang. Hear. Res.* 57, 1619–1637. doi: 10.1044/2014_JSLHR-S-12-0405
- Scherer, R. C., Shinwari, D., De Witt, K. J., Zhang, C., Kucinski, B. R., and Afjeh, A. A. (2001). Intraglottal pressure profiles for a symmetric and oblique glottis with a divergence angle of 10 degrees. *J. Acoust. Soc. Am.* 109, 1616–1630. doi: 10.1121/1.1333420
- Schneider, B., and Bigenzahn, W. (2003). Influence of glottal closure configuration on vocal efficacy in young normal-speaking women. *J. Voice* 17, 468–480. doi: 10.1067/S0892-1997(03)00065-1
- Schoder, S., Junger, C., Weitz, M., and Kaltenbacher, M. (2019). “Conservative source term interpolation for hybrid aeroacoustic computations,” in *25th AIAA/CEAS Aeroacoustics Conference, 2019* (Delft: American Institute of Aeronautics and Astronautics Inc., AIAA). doi: 10.2514/6.2019-2538
- Schoder, S., Weitz, M., Maurerlehner, P., Hauser, A., Falk, S., Kaltenbacher, M., et al. (2020). Hybrid aeroacoustic approach for the efficient numerical simulation of human phonation. *J. Acoust. Soc. Am.* 147, 1179–1194. doi: 10.1121/10.0000785
- Schuberth, S., Hoppe, U., Döllinger, M., Lohscheller, J., and Eysholdt, U. (2002). High-precision measurement of the vocal fold length and vibratory amplitudes. *Laryngoscope* 112, 1043–1049. doi: 10.1097/00005537-200206000-00020
- Sciamarella, D., and Le Quéré, P. (2008). Solving for unsteady airflow in a glottal model with immersed moving boundaries. *Eur. J. Mech.* 27, 42–53. doi: 10.1016/j.euromechflu.2007.06.004
- Semmler, M., Döllinger, M., Patel, R. R., Ziethe, A., and Schützenberger, A. (2018). Clinical relevance of endoscopic three-dimensional imaging for quantitative assessment of phonation. *Laryngoscope* 128, 2367–2374. doi: 10.1002/lary.27165

- Södersten, M., Hertegard, S., and Hammarberg, B. (1995). Glottal closure, translottal airflow, and voice quality in healthy middle-aged women. *J. Voice* 9, 182–197. doi: 10.1016/S0892-1997(05)80252-8
- Södersten, M., and Lindestad, P. Å. (1990). Glottal closure and perceived breathiness during phonation in normally speaking subjects. *J. Speech Lang. Hear. Res.* 33, 601–611. doi: 10.1044/jshr.3303.601
- Story, B. H., Titze, I. R., and Hoffman, E. A. (1996). Vocal tract area functions from magnetic resonance imaging. *J. Acoust. Soc. Am.* 100, 537–554. doi: 10.1121/1.415960
- Sundberg, J., Fahlstedt, E., and Morell, A. (2005). Effects on the glottal voice source of vocal loudness variation in untrained female and male voices. *J. Acoust. Soc. Am.* 117, 879–885. doi: 10.1121/1.1841612
- Sundberg, J., Titze, I., and Scherer, R. (1993). Phonatory control in male singing: a study of the effects of subglottal pressure, fundamental frequency, and mode of phonation on the voice source. *J. Voice* 7, 15–29. doi: 10.1016/S0892-1997(05)80108-0
- Tanaka, S., and Gould, W. J. (1985). Vocal efficiency and aerodynamic aspects in voice disorders. *Ann. Otol. Rhinol. Laryngol.* 94, 29–33. doi: 10.1177/000348948509400107
- Tao, C., and Jiang, J. J. (2008). A self-oscillating biophysical computer model of the elongated vocal fold. *Comput. Biol. Med.* 38, 1211–1217. doi: 10.1016/j.compbiomed.2008.10.001
- Taylor, C. J., Tarbox, G. J., Bolster, B. D., Bangerter, N. K., and Thomson, S. L. (2019). Magnetic resonance imaging-based measurement of internal deformation of vibrating vocal fold models. *J. Acoust. Soc. Am.* 145, 989–997. doi: 10.1121/1.5091009
- Thomson, S. L., Mongeau, L., and Frankel, S. H. (2005). Aerodynamic transfer of energy to the vocal folds. *J. Acoust. Soc. Am.* 118, 1689–1700. doi: 10.1121/1.2000787
- Thornton, F., Döllinger, M., Kniesburges, S., Berry, D., Alexiou, C., and Schützenberger, A. (2019). Impact of subharmonic and aperiodic laryngeal dynamics on the phonatory process analyzed in *ex vivo* rabbit models. *Appl. Sci.* 9, 1–18. doi: 10.3390/app9091963
- Titze, I. R. (1992). Vocal efficiency. *J. Voice* 6, 135–138. doi: 10.1016/S0892-1997(05)80127-4
- Titze, I. R. (2000). *Principles of Voice Production*. Iowa City, IA: National Center of Voice and Speech.
- Titze, I. R., Maxfield, L., and Palaparthi, A. (2016). An oral pressure conversion ratio as a predictor of vocal efficiency. *J. Voice* 30, 398–406. doi: 10.1016/j.jvoice.2015.06.002
- Vaca, M., Cobeta, I., Mora, E., and Reyes, P. (2017). Clinical assessment of glottal insufficiency in age-related dysphonia. *J. Voice* 31:128.e1–128.e5. doi: 10.1016/j.jvoice.2015.12.010
- van den Berg, J., Zantema, J. T., and Doornenbal, P. (1957). On the air resistance and the bernoulli effect of the human larynx. *J. Acoust. Soc. Am.* 29, 626–631. doi: 10.1121/1.1908987
- Van Hirtum, A., and Pelorson, X. (2017). High-speed imaging to study an auto-oscillating vocal fold replica for different initial conditions. *Int. J. Appl. Mech.* 9:1750064. doi: 10.1142/S1758825117500648
- Xue, Q., Mittal, R., Zheng, X., and Bielamowicz, S. (2010). A computational study of the effect of vocal-fold asymmetry on phonation. *J. Acoust. Soc. Am.* 128, 818–827. doi: 10.1121/1.3458839
- Xue, Q., Zheng, X., Mittal, R., and Bielamowicz, S. (2014). Subject-specific computational modeling of human phonation. *J. Acoust. Soc. Am.* 135, 1445–1456. doi: 10.1121/1.4864479
- Yamauchi, A., Yokonishi, H., Imagawa, H., Sakakibara, K.-i., Nito, T., Tayama, N., et al. (2014). Age- and gender-related difference of vocal fold vibration and glottal configuration in normal speakers: analysis with glottal area waveform. *J. Voice* 28, 525–531. doi: 10.1016/j.jvoice.2014.01.016
- Yamauchi, A., Yokonishi, H., Imagawa, H., Sakakibara, K. I., Nito, T., Tayama, N., et al. (2016). Quantification of vocal fold vibration in various laryngeal disorders using high-speed digital imaging. *J. Voice* 30, 205–214. doi: 10.1016/j.jvoice.2015.04.016
- Zañartu, M., Galindo, G. E., Erath, B. D., Peterson, S. D., Wodicka, G. R., and Hillman, R. E. (2014). Modeling the effects of a posterior glottal opening on vocal fold dynamics with implications for vocal hyperfunction. *J. Acoust. Soc. Am.* 136, 3262–3271. doi: 10.1121/1.4901714
- Zhang, Y., Jiang, W., Sun, L., Wang, J., Smith, S., Titze, I. R., et al. (2020). A deep-learning based generalized reduced-order model of glottal flow during normal phonation. *arXiv preprint arXiv:2005.11427*.
- Zhang, Z. (2019). Compensation strategies in voice production with glottal insufficiency. *J. Voice* 33, 96–102. doi: 10.1016/j.jvoice.2017.10.002
- Zhang, Z. (2020). Estimation of vocal fold physiology from voice acoustics using machine learning. *J. Acoust. Soc. Am.* 147, EL264–EL270. doi: 10.1121/10.0000927
- Zhang, Z., Kreiman, J., Gerratt, B. R., and Garellek, M. (2012). Acoustic and perceptual effects of changes in body layer stiffness in symmetric and asymmetric vocal fold models. *J. Acoust. Soc. Am.* 133, 453–462. doi: 10.1121/1.4770235
- Zhang, Z., Mongeau, L., Frankel, S. H., Thomson, S., and Park, J. B. (2004). Sound generation by steady flow through glottis-shaped orifices. *J. Acoust. Soc. Am.* 116, 1720–1728. doi: 10.1121/1.1779331
- Zhang, Z., and Mongeau, L. G. (2006). Broadband sound generation by confined pulsating jets in a mechanical model of the human larynx. *J. Acoust. Soc. Am.* 119, 3995–4005. doi: 10.1121/1.2195268
- Zörner, S., Kaltenbacher, M., and Döllinger, M. (2013). Investigation of prescribed movement in fluid-structure interaction simulation for the human phonation process. *Comput. Fluids* 86, 133–140. doi: 10.1016/j.compfluid.2013.06.031
- Zörner, S., Šidlof, P., Hüppe, A., and Kaltenbacher, M. (2016). Flow and acoustic effects in the larynx for varying geometries. *Acta Acust. United Acust.* 102, 257–267. doi: 10.3813/AAA.918942

Conflict of Interest: The authors declare that the research was conducted in the absence of any commercial or financial relationships that could be construed as a potential conflict of interest.

Copyright © 2021 Falk, Kniesburges, Schoder, Jakubaß, Maurerlehner, Echternach, Kaltenbacher and Döllinger. This is an open-access article distributed under the terms of the Creative Commons Attribution License (CC BY). The use, distribution or reproduction in other forums is permitted, provided the original author(s) and the copyright owner(s) are credited and that the original publication in this journal is cited, in accordance with accepted academic practice. No use, distribution or reproduction is permitted which does not comply with these terms.